J|A|C|S
ARTICLES
Published on Web 01/26/2002

A New Class of Functionalized Terpyridyl Ligands as Building Blocks for Photosensitized Supramolecular Architectures. Synthesis, Structural, and Electronic Characterizations

Philippe Lainé,*,† Fethi Bedioui,‡ Philippe Ochsenbein,⊥,§ Valérie Marvaud,|| Michel Bonin,§ and Edmond Amouyal†

Contribution from the Laboratoire de Chimie Physique, CNRS UMR 8000, Université Paris-Sud, Bâtiment 350, 91405 Orsay Cedex, France, Laboratoire d'Électrochimie et Chimie Analytique, CNRS UMR 7575, École Nationale Supérieure de Chimie de Paris, 11 rue Pierre et Marie Curie, 75231 Paris Cedex 05, France, Sanofi-Synthélabo Recherche, 371 rue du Professeur Blayac, 34184 Montpellier Cedex 04, France, Laboratoire de Chimie Inorganique et Matériaux Moléculaires, CNRS UMR 7071, Université Pierre et Marie Curie, 4 Place Jussieu, F-75252 Paris Cedex 05, France, and Institute of Crystallography, University of Lausanne, BSP, 1015 Lausanne, Switzerland

Received April 27, 2001

Abstract: A new class of triarylpyridinio-derivatized [4′-(*p*-phenyl)$_n$]terpyridyl ligands, $R^1{}_2R^2TP^+$-(p)$_n$tpy, was designed as a novel category of electron-acceptor (A)-substituted *proto*-photosensitizing molecules. The first elements of this versatile family of ligands (i.e., $n = 0$, 1 and $R^1 = R^2 = H$), H_3TP^+-tpy and H_3TP^+-ptpy, were synthesized as well as their Ru(II) and Os(II) complexes to form the related acceptor-functionalized $M(tpy)_2{}^{2+}$ and $M(ptpy)_2{}^{2+}$ photosensitizer components denoted P0 and P1, respectively. Within the P1 series of compounds, an electron-donor (D)-substituted ligand, Me_2N-ptpy, was also involved and associated with H_3TP^+-ptpy, giving rise to various combinations (up to 10 polyad systems). The two resulting series of nanometer-scale rigid rod-like photosensitized supramolecular architectures are of potential interest for long-range photoinduced electron transfer purposes. The main structural features of such supermolecules were determined by comparing the results obtained from (i) single-crystal X-ray analysis of the two free ligands together with that of the **P0A/Ru** and **P1A$_2$/Ru** complexes and (ii) a detailed solution ^{1}H NMR study of the P0 series and, more specifically, of the **P0A/Ru** dyad (ROESY experiment). It is shown that the pseudoperpendicular conformation of the covalently linked A and P subunits found in the solid state is persistent in fluid medium; i.e., A is not conjugated with P (P0 and P1). The first insights regarding the consequences upon intercomponent couplings of combined substituent effects and conjugation (case of D-based polyads)—or absence of conjugation—are discussed in the light of ground-state electronic properties of the compounds.

1. Introduction

Molecular electronics and artificial photosynthesis are closely related challenging fields of research that have experienced a considerable rise during the last few decades. These noticeable advances partly originated in the advent of new insights in molecular chemistry,[1] along with the revival of inorganic photochemistry.[2]

Originally concerned with weakly interacting individual molecules, the concepts of supramolecular chemistry[3] have readily spread around toward *covalently* assembled architectures, the latter "*molecules*" being therefore viewed as the full *building blocks* of a final *supermolecule*.[1a] From the point of view of physical chemists, the supermolecule is thus proposed to be a multicomponent system (polyad) which behaves as a small device capable of performing a predetermined function, i.e., of receiving an external stimulus (input) and specifically reacting (output). A significant feature of such supermolecules, examined in the ground state, stems from the fact that the parentage of each component remains identifiable with respect to the corresponding isolated entities. In other words, the constitutive subunits are not being too strongly coupled one to the others.[4,5] Thus, depending on the intrinsic properties of the associated units, the resulting assembly may achieve various *functions*.

† Université Paris-Sud.
‡ École Nationale Supérieure de Chimie de Paris.
⊥ Present address: Sanofi-Synthélabo Recherche.
|| Université Pierre et Marie Curie.
§ University of Lausanne.

(1) (a) Lehn, J.-M. *Angew. Chem., Int. Ed. Engl.* **1988**, *27*, 89−112. (b) Aviram, A.; Ratner, M. A. *Chem. Phys. Lett.* **1974**, *29*(2), 277−283.
(2) (a) Meyer, T. J. *Acc. Chem. Res.* **1989**, *22*(5), 163−170. (b) Juris, A.; Balzani, V.; Barigelletti, F.; Belser, P.; Von Zelewsky, A. *Coord. Chem. Rev.* **1988**, *84*, 85−277.
(3) Lehn, J.-M. *Pure Appl. Chem.* **1978**, *50*, 871−892.
(4) (a) Balzani, V.; Juris, A.; Venturi, M.; Campagna, S.; Serroni, S. *Chem. Rev.* **1996**, *96*, 759−833. (b) Balzani, V.; Moggi, L.; Scandola, F. In *Supramolecular Photochemistry*; Balzani, V., Ed; D. Reidel Publishing Co.: Dordrecht, The Netherlands, 1987; pp 1−28. (c) Balzani, V.; Scandola, F. *Supramolecular Photochemistry*; Ellis Horwood: Chichester, 1991.
(5) Sauvage, J.-P.; Collin, J.-P.; Chambron, J.-C.; Guillerez, S.; Coudret, C.; Balzani, V.; Barigelletti, F.; De Cola, L.; Flamigni, L. *Chem. Rev.* **1994**, *94*, 993−1019 and references therein.

10.1021/ja011069p CCC: $22.00

When light is the primary efficient stimulus (photosensitized species), photochemical molecular devices (PMDs)[4b,c,5,6] are concerned, and one of the most investigated light-triggered functions at the molecular level is undoubtedly the monitoring of photoinduced electron transfer (PET) processes. These phenomena are of fundamental importance within the framework of research devoted to molecular electronics[4−7] and solar energy photoconversion and storage.[2a,8] A typical composition of supramolecular species built for such purposes consists of electron-donating (D) and/or -accepting (A) units, associated with a photosensitizer (P) that exhibits substantial redox activity at the excited state. When designed more specifically for artificial photosynthesis, these electroactive entities are assembled within the polyad systems in such a manner that sequential intramolecular electron transfers (ETs) following the excitation of P lead to a charge-separated (CS) state (e.g., D^+-P-A^-). This CS state actually corresponds to the transient conversion of light into an electrochemical potential that may be subsequently used—under appropriate conditions—for performing chemistry (fuel, energy storage) or producing electricity.[9] Depending on whether the final goal is related to molecular electronics or artificial photosynthesis, the supramolecular species will be rather tuned in order to get a fast and long-range ET (e.g., nanometer-scale electron wires) or long-life CS state, respectively. Hence, it is of determining importance to design supramolecular architectures allowing fine control over both the properties of their components and their overall geometrical features.

Over the years, topological, thermodynamic, and kinetic criteria that govern PET processes within polyad systems have been determined and the components satisfying these requirements progressively selected.[4a,c,5] Metalated and nonmetalated porphyrins together with d^6 transition metal complexes (second and third rows) with oligopyridyl ligands are among the most popular chromophoric photosensitizers, P.[2b,4,5,10] Concerning the other ingredients (D, A) of the multicomponent systems, substituted amines, phenothiazines, and carotenoid polyenes are commonly employed as electron-releasing elements, whereas naphthalenediimide fragments, dicyanovinyl groups, fullerenes, and more notably quinones and bipyridinium (viologens) species generally play the role of electron-withdrawing units.[2a,5,8,11] Although viologens are somewhat archetypal as organic electron-acceptor building blocks, there exists, however, a class of pyridinium species less frequently used, namely the *N*-aryl-substituted pyridinio derivatives. Interestingly, this type of monopyridinium fragment has already been involved as the electron-acceptor moiety in a family of purely organic bipartite molecules which undergo intramolecular charge transfers. These zwitterionic compounds are the solvatochromic pyridinium *N*-phenolate betaine dyes (so-called Reichardt's salt), widely adopted as solvent polarity indicators.[12] In addition, the structure of such a pyridinium moiety can be extensively varied in order to give different—but affiliated—dyes, thus allowing the probing of almost all solvents at our disposal.[13] It is worth noting that this synthetic versatility of *N*-aryl pyridinio molecules actually originates from that of their pyrylium precursors (Chart 1). Indeed, the pyrylium ring can be substituted almost on demand; fortunately, its chemistry is also well-established and documented.[14]

Chart 1

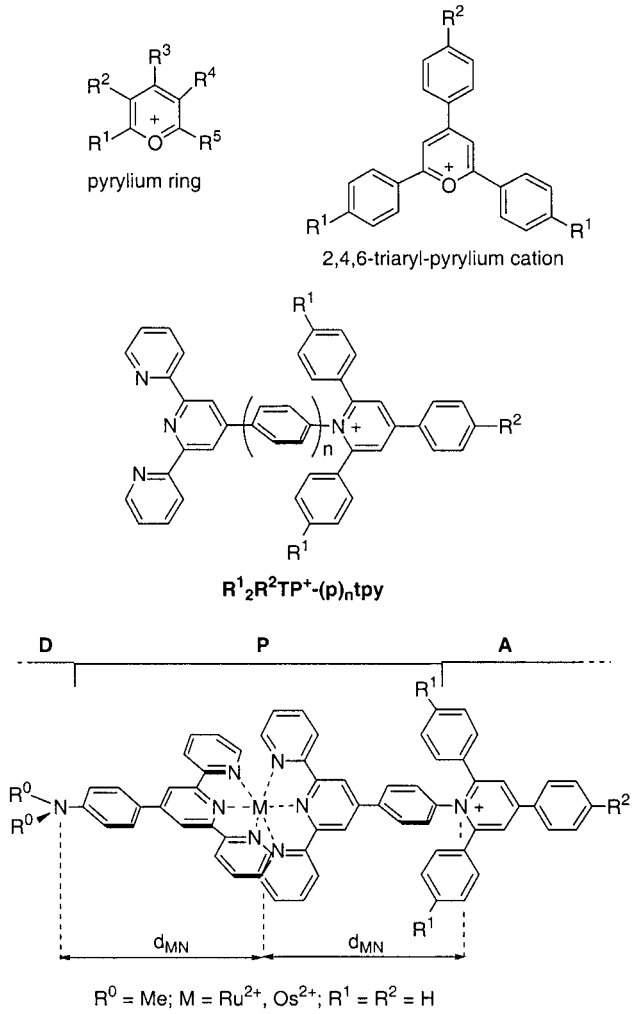

As part of our work devoted to the search for new building blocks for inorganic PMDs of potential interest for energy conversion or information storage purposes, our proposal is thus

(6) Lehn, J.-M. *Angew. Chem., Int. Ed. Engl.* **1990**, *29*, 1304−1319.
(7) (a) Joachim, C.; Gimzeswski, J. K.; Aviram, A. *Nature* **2000**, *408*, 541−548. (b) *Molecular Electronics, Science and Technology*; Aviram, A., Ed.; American Institute of Physics: New York, 1992. (c) *Molecular Electronics*; Launay, J.-P., Ed. *New J. Chem.* **1991**, *15* (special issue).
(8) (a) Gust, D.; Moore, T. A.; Moore, A. L. *Acc. Chem. Res.* **2001**, *34*, 40−48. (b) Amouyal, E. In *Homogeneous Photocatalysis*; Chanon, M., Ed.; John Wiley: Chichester, 1997; Chapter 8, pp 263−307. (c) Barbara, P. F.; Meyer, T. J.; Ratner, M. A. *J. Phys. Chem.* **1996**, *100*, 13148−13168. (d) Hagfeldt, A.; Grätzel, M. *Chem. Rev.* **1995**, *95*, 49−68. (e) Bard, A. J.; Fox, M. A. *Acc. Chem. Res.* **1995**, *28*, 141−145. (f) Amouyal, E. *Sol. Energy Mater. Sol. Cells.* **1995**, *38*, 249−276. (g) Paddon-Row, M. N. *Acc. Chem. Res.* **1994**, *27*, 18−25. (h) Wasielewski, M. R. *Chem. Rev.* **1992**, *92*, 435−461. (i) Gust, D.; Moore, T. A.; Moore, A. L. *Acc. Chem. Res.* **1993**, *26*, 198−205. (j) *Photoinduced Electron Transfer*; Fox, M. A., Chanon, M., Eds.; Elsevier: Amsterdam, 1988.
(9) (a) Imahori, H.; Norieda, H.; Yamada, H.; Nishimura, Y.; Yamazaki, I.; Sakata, Y.; Fukuzumi, S. *J. Am. Chem. Soc.* **2001**, *123*, 100−110. (b) Hagfeldt, A.; Grätzel, M. *Acc. Chem. Res.* **2000**, *33*, 269−277. (c) Bignozzi, C. A.; Argazzi, R.; Indelli, M. T.; Scandola, F. *Sol. Energy Mater. Sol. Cells* **1994**, *32*, 229−244. (d) O'Regan, B.; Grätzel, M. *Nature* **1991**, *353*, 737−740.
(10) Kalyanasundaram, K. *Photochemistry of Polypyridine and Porphyrin Complexes*; Academic Press: London, 1992.
(11) Imahori, H.; Sakata, Y. *Eur. J. Org. Chem.* **1999**, 2445−2457 and references therein.
(12) (a) Reichardt, C. *Chem. Rev.* **1994**, *94*, 2319−2358 and references therein. (b) Chen, P.; Meyer, T. J. *Chem. Rev.* **1998**, *98*, 1439−1477.
(13) Dimroth, K.; Reichardt, C.; Siepmann, T.; Bohlmann, F. *Liebigs Ann. Chem.* **1963**, *661*, 1−37.
(14) Balaban, A. T.; Dinculescu, A.; Dorofeyenko, G. N.; Fischer, G. W.; Koblik, V. V.; Mezheritskii, A. V.; Schroth, W. In *Pyrylium Salts: Synthesis, Reactions and Physical Properties. Advances in Heterocyclic Chemistry*; Katritzky, A. R., Ed.; Academic Press: New York, 1982; Suppl. 2.

to take advantage of the properties of these latter *N*-aryl-substituted pyridinio electron-accepting groups by replacing, in the case of polypyridyl complexes of Ru(II) and Os(II), the phenolate organic moiety of betaine dyes by light-triggered electron donors. Based on hitherto established structural and energetic requirements, the new 4′-[4-*N*-(2,4,6-triarylpyridinio)-phenyl]-2,2′:6′,2″-terpyridine ligand ($R^1_2R^2TP^+$-ptpy) has been designed,[15] as well as the directly functionalized analogue 4′-*N*-(2,4,6-triarylpyridinio)-2,2′:6′,2″-terpyridine ($R^1_2R^2TP^+$-tpy) depicted in Chart 1. The only difference between these two ligands stems from the presence of a phenyl spacer (p) that allows an increase of the intercomponent distance without any loss regarding the main topological features (axial symmetry, rigidity, ...) of the resulting complexes. In addition, such a connector can be equally intercalated between P and A/D electroactive units for both the triarylpyridinio electron-acceptor moiety and electron-releasing groups such as NR_2 (R = alkyl, aryl) to form donor-substituted ligands of the type of 4′-(4-*N*,*N*-disubstituted-aminophenyl)tpy (R_2N-ptpy, R = alkyl, aryl) (Chart 1).[15] When these two types of ligands are associated within the same heteroleptic complexes, the resulting triads, D−P−A, exhibit a supplementary interesting characteristic for CS purposes. Indeed, both pyridinio and amino nitrogen atoms are located at equal distances d_{MN} from the metal center (M) (Chart 1), which may favor a competition between intramolecular ETs, thus retarding the charge recombination.[5,15]

The main features of these novel triarylpyridinium-derivatized terpyridyl ligands are their well-defined topology (rigid structures) and their chemical flexibility. Thus, it is expected that the electronic and redox properties of the acceptor moieties could be tuned via peripheral substituents (R^1 and R^2). Regarding the connectivity of the complexes, the structure could be expanded either via R^2 to give rise to singly linked axial rods of adjustable length,[5,16] so as to generate long-range vectorial ET (electron wires) and long-lived CS, or via both R^1 and R^2 in order to build branched architectures (antenna effects, multielectron catalysis, "molecular batteries").[17]

As a prerequisite for manipulating such potentially complex supramolecular architectures, a detailed study of the original skeleton ($R^1_2R^2TP^+$-$(p)_n$tpy, $R^1 = R^2 = H$ and $n = 0, 1$) is required in order to establish forthcoming and possibly related complicated chemistry. Our approach is aimed at reporting on the very basic properties and main features of the native building blocks, before their modification to explore new potentialities.[15] In this work, the new families of ruthenium(II) and osmium(II) complexes with triphenylpyridinio-derivatized electron-acceptor ligands are presented and fully characterized. The dimethylamino-substituted *p*-phenyl-terpy is also described. It has been used for illustration purposes as a representative element of the family of the donor ligands (R_2N-ptpy) that may be suitably associated with the $R^1_2R^2TP^+$-ptpy partners, although such dimethyl derivative may not be the best candidate as electron-donor (vs *P). This study is indeed mainly focused on the analysis of the influence of the novel *acceptor*-derivatized ligands upon P, the effects of the donor ligand being also investigated as they give some insights (especially concerning the electronic coupling between P and D) that remain valid for the other elements of the R_2N-ptpy family. Of importance, *the structural aspect* is more specifically addressed here, as it is related to the actual electronic coupling between P and A. Indeed, the cost for the rigidity of the overall architecture is potentially the partial conjugation of A with P, which can be considered as a drawback for charge-separation purposes and for PMDs, as defined within the framework of supramolecular photochemistry.

2. Results and Discussion

2.1. Synthesis. The key intermediate for the synthesis of $R^1_2R^2TP^+$-substituted ligands is the amino derivative of their chelating fragment. Actually, despite the wide variety of reactions that may be subsequently performed on such a starting material, the synthesis of amino-terpyridine ligands has only recently attracted its merited interest. In an effort to synthesize the H_3TP^+-tpy ligand, we have thus undertaken the preparation of the 4′-amino-2,2′:6′,2″-terpyridine (H_2N-tpy), by using the Stille coupling reaction,[18] in accordance with a strategy adapted from that first reported by Yamamoto et al. for the synthesis of some other terpyridines (Scheme 1).[19] In the meantime, Fallahpour and co-workers[20] described a synthesis of the target amino precursor, following a procedure very similar to ours. We will therefore refer to their published synthetic route for the preparation of the key H_2N-tpy molecule.

Regarding the 4′-[*p*-aminophenyl]-2,2′:6′,2″-terpyridine (H_2N-ptpy) precursor, syntheses different from that we have selected were also recently reported in the literature.[21] Instead of directly synthesizing the H_2N-ptpy ligand from polymerized *p*-aminobenzaldehyde and 2-acetylpyridine, a two-step synthesis via the nitro intermediate was preferred (also because of our need of this latter compound for other purposes). Thus, the synthetic route (Scheme 1) consists first of preparing the 4′-[*p*-nitrophenyl]terpy according to a procedure adapted from that reported by Collin et al. for making the 4′-*p*-tolyl-terpy (ttpy or Me-ptpy)[22] and based on the conventional one-pot synthesis of 4′-[*para*-substituted phenyl]-terpy ligands.[23] The purification was then performed by the method of Constable et al.[22,24] The nitro species was subsequently converted into the corresponding amino derivative with hydrazine over palladium charcoal[25] (quantitative reaction) with an overall yield of ca. 10.5% (steps viii and vi, Scheme 1). Note that the reduction of the nitro group was *in fine* preferably performed with hydrazine on palladium charcoal rather than with sodium dithionite[15] of irregular and lower efficiency. Moreover, high yields for the reduction reaction are of crucial importance when several nitro groups belonging to the same molecule have to be transformed to obtain branched species.

(15) Lainé, P.; Amouyal, E. *Chem. Commun*. **1999**, 935−936.
(16) (a) Swiegers, G. F.; Malefetse, T. J. *Chem. Rev*. **2000**, *100*, 3483−3537. (b) Schwab, P. F. H.; Levin, M. D.; Michl, J. *Chem. Rev*. **1999**, *99*, 1863−1933. (c) Collin, J.-P.; Gaviña, P.; Heitz, V.; Sauvage, J.-P. *Eur. J. Inorg. Chem*. **1998**, 1−14. (d) Barigelletti, F.; Flamigni, L.; Collin, J.-P.; Sauvage, J.-P. *Chem. Commun*. **1997**, 333−338.
(17) (a) Kimura, M.; Shiba, T.; Muto, T.; Hanabusa, K.; Shirai, H. *Chem. Commun*. **2000**, 11−12. (b) Mayor, M.; Lehn, J.-M. *J. Am. Chem. Soc*. **1999**, *121*, 11231−11232. (c) Astruc, D. *Electron Transfer and Radical Processes in Transition-Metal Chemistry*; VCH: New York, 1995.
(18) Stille, J. K. *Angew. Chem., Int. Ed. Engl*. **1986**, *25*, 508−524.
(19) Yamamoto, Y.; Azuma, Y.; Mitoh, H. *Synthesis* **1986**, 564−565.
(20) (a) Fallahpour, R.-A. *Eur. J. Inorg. Chem*. **1998**, 1205−1207. (b) Fallahpour, R.-A.; Neuburger, M.; Zehnder, M. *New J. Chem*. **1999**, 53−61 and references therein.
(21) Storrier, G. D.; Colbran, S. B.; Craig, D. C. *J. Chem. Soc., Dalton Trans*. **1997**, 3011−3028.
(22) Collin, J.-P.; Guillerez, S.; Sauvage, J.-P.; Barigelletti, F.; De Cola, L.; Flamigni, L.; Balzani, V. *Inorg. Chem*. **1991**, *30*, 4230−4238.
(23) Spahni, W.; Calzaferri, G. *Helv. Chim. Acta* **1984**, *67*, 450−454.
(24) Constable, E. C.; Ward, M. D.; Corr, S. *Inorg. Chim. Acta* **1988**, *141*, 201−203.
(25) Black, D. St. C.; Rothnie, N. E. *Aust. J. Chem*. **1983**, *36*, 1141−1147.

Scheme 1. Synthetic Routes for the Novel Triphenylpyridinio-Substituted Terpyridyl Ligands and Numbering Scheme Adopted for ^{1}H and ^{13}C NMR Assignments[a]

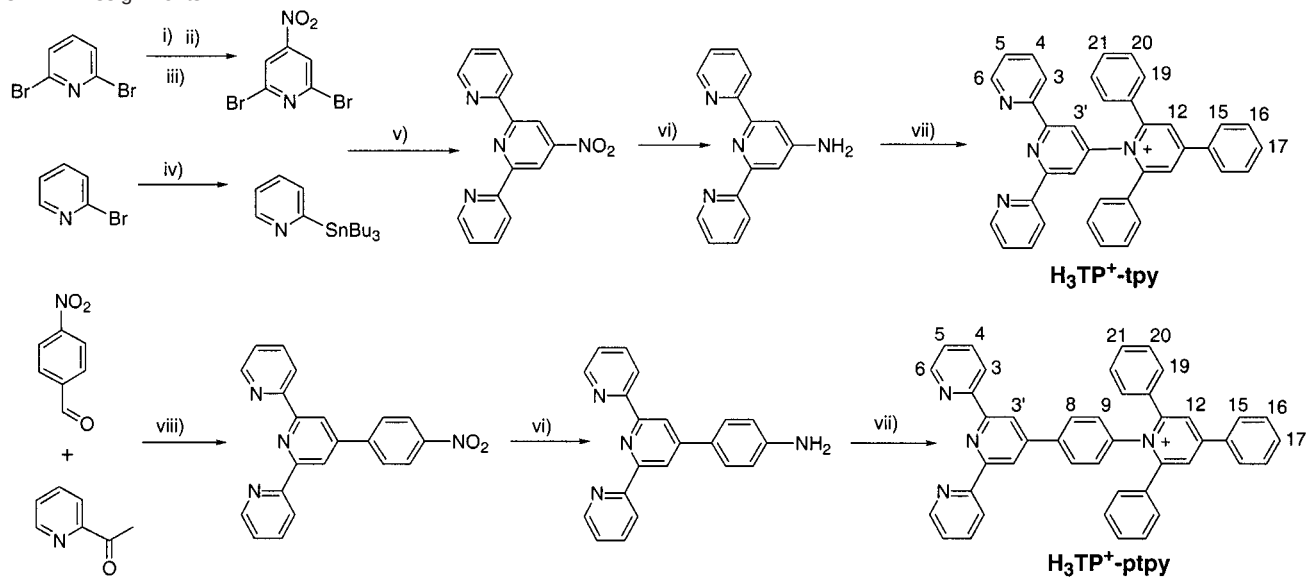

[a] Reagents and conditions: (i) H_2O_2/TFA. (ii) HNO_3/H_2SO_4. (iii) $CHCl_3/PCl_3$. (iv) nBuLi, Bu_3SnCl, THF, −78 °C. (v) $Pd(PPh_3)_4$, toluene, T°. (vi) Pd/C (10%), EtOH, $H_2NNH_2{\cdot}H_2O$, T°. (vii) pyrylium salt, NaOAc/EtOH, T°. (viii) NH_4OAc, CH_3CONH_2, T°; NaOH aq, T°; $[Fe^{2+}]$, $NaOH/H_2O_2$.

The last step for the preparation of the pyridinium moieties was adapted from the synthesis of the Betaine 30 solvatochromic dye.[13,26] H_3TP^+-tpy and H_3TP^+-ptpy ligands were synthesized by reacting the related amino precursor with the commercially available triphenylpyrylium salt, affording the target molecules as salts (Scheme 1). It is worth emphasizing, in view of forthcoming works, that the very well documented chemistry of triarylpyrylium organic material[14] is such that it offers a wide variety of possible designs for pyridinio-derivatized ligands.[27] One should also underline the stability of the new synthesized ligands. Indeed, although triphenylpyrylium salts are often used for functional group conversion purposes,[28] as is the case for primary alkyl and benzylamines which are converted into their corresponding pyridinium leaving groups,[29] *N-arylpyridinium salts normally do not undergo nucleophilic displacement reactions*.[29] The two reported exceptions are dealing with cases where pyrolysis at a temperature above 200 °C or thermolysis above 220 °C was performed.[30] The chemical inertness of the *N*-arylpyridinio derivatives is explained by the fact that stereoelectronic requirements for intermolecular nucleophilic displacements of *N*-aryl groups are not favorable (steric protection of the α substituents of the pyridinium ring).[30]

The synthetic route for the model electron-donor ligand, Me_2N-ptpy, was adapted from that previously mentioned for NO_2-ptpy,[22] by reacting 2-acetylpyridine with the conveniently substituted aldehyde, i.e., *p-N,N*-dimethylamino benzaldehyde.

Homoleptic complexes, $[(L)_2M]^{n+}$ ($n = 2, 4$), were directly synthesized by reacting the transition metal chloride ($MCl_3{\cdot}3H_2O$, M = Ru, Os) with the corresponding ligand (L) in approximately stoichiometric proportions (i.e., 1:2 respectively, with a slight excess for L). The syntheses were performed in the presence of sodium ascorbate as a reducing agent, instead of the generally used *N*-ethylmorpholine or triethylamine, because of the additional moderate complexing property of ascorbate that may help in the displacement of chloride anions from MCl_3. Heteroleptic complexes, $[(L^1)M(L^2)]^{n+}$ ($n = 2, 3$), were obtained in two steps by reacting first the ligand L^1 with the metal trichloride to get the poorly soluble neutral complex $(L^1)MCl_3$, and then this latter precursor with the second ligand (L^2) in the same conditions as for the synthesis of the homoleptic compounds. All cationic complexes were first purified by counteranion metathesis ($Cl^- \rightarrow PF_6^-$) and then by column chromatography over basic alumina. The final recrystallization of the pure product was usually accomplished by slow vapor diffusion of diethyl ether into an acetonitrile solution of the complex. All complexes synthesized, along with their corresponding labels, are schematically gathered in Chart 2. Homoleptic complexes have been synthesized as reference compounds for comparison purposes.

Chart 2. Schematic Structures of the Polyad Systems with Their Corresponding Label (In All Cases the Counterions Are PF_6^-)

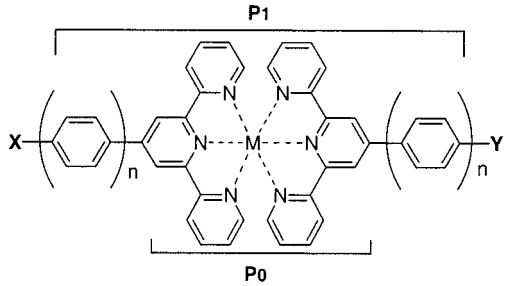

n = 0 and M = Ru^{2+}		n = 1 and M = Ru^{2+}, Os^{2+}	
P0	**X** = **Y** = H	**P1**	**X** = **Y** = Me
P0A$_2$	**X** = **Y** = H_3TP^+	**P1A$_2$**	**X** = **Y** = H_3TP^+
P0A	**X** = H and **Y** = H_3TP^+	**P1A**	**X** = Me and **Y** = H_3TP^+
		D$_2$P1	**X** = **Y** = Me_2N
		DP1	**X** = Me_2N and **Y** = Me
		DP1A	**X** = Me_2N and **Y** = H_3TP^+

(26) (a) Kessler, M. A.; Wolfbeis, O. S. *Synthesis* **1988**, 635−636. (b) Osterby, B. R.; McKelvey, R. D. *J. Chem. Educ*. **1996**, *73*, 260−261.
(27) Work in progress.
(28) *Vogel's Textbook of Practical Organic Chemistry*, 5th ed; Furniss, B. S., Hannaford, A. J., Smith, P. W. G., Tatchell, A. R., Eds.; John Wiley & Sons: New York, 1989.
(29) Katritzky, A. R. *Tetrahedron* **1980**, *36*, 679−699.
(30) Katritzky, A. R.; Marson, C. *Angew. Chem., Int. Ed. Engl*. **1984**, *23*, 420−429.

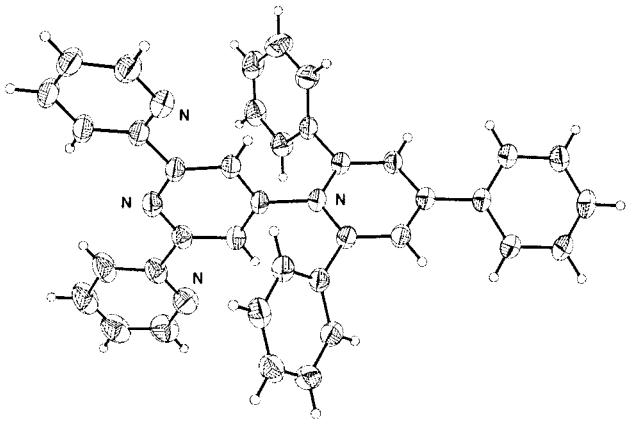

Figure 1. ORTEP drawing of the H_3TP^+-tpy ligand with thermal ellipsoids (50% probability). The BF_4^- counterion and the cocrystallized solvent molecule are omitted for clarity.

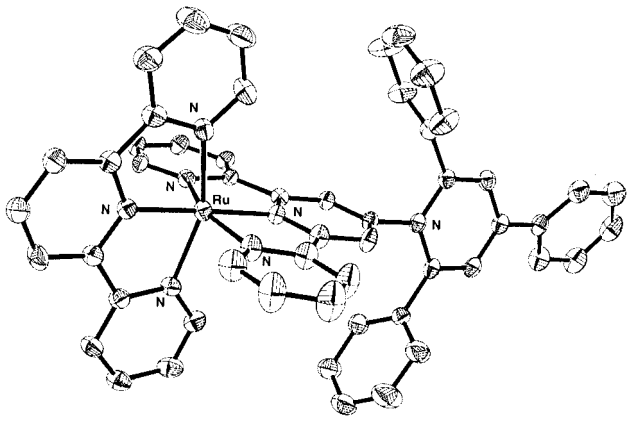

Figure 2. ORTEP drawing of the $[(tpy)Ru(tpy\text{-}TPH_3^+)]^{3+}$ complex, **P0A/Ru**, with thermal ellipsoids (30% probability). The hydrogen atoms, PF_6^- counterions, and cocrystallized solvent molecules are omitted for clarity.

The purity of all compounds and their identity (for the new species) were checked by elemental analysis, ^1H and ^{13}C NMR, and CI and ES mass spectrometry, and they are in good agreement with the expected structures. However, it should be noted that the elemental analysis of H_3TP^+-phenyl and -ptpy derivatives indicates that partial to almost complete anion-exchange did take place between that coming from the pyrylium source (HSO_4^-) and that coming from the sodium salt (OAc^-) present in excess in the reaction medium during the last step of pyridinium formation. This may account for the poor crystal quality of the H_3TP^+-ptpy ligand, which showed unresolved disorder regarding the counterion (see below). We did not perform any further metathesis on the mixed (HSO_4^-/OAc^-) salts of the ligands, which were used as obtained for the following step of complexation, affording pure PF_6^- salts after purification. Fortunately, this untimely ion exchange did not occur when the BF_4^- salt of the pyrylium precursor was used, as was the case for the $[H_3TP^+\text{-tpy}](BF_4)$ ligand, which was readily crystallized in a pure form. Concerning the microanalytical results for the inorganic compounds, it was observed that the experimentally determined carbon abundance was, from time to time, lower than that expected theoretically. This finding has already been reported and ascribed to the propensity of Ru (and Os) transition metals to form carbides species upon combustion.[31]

2.2. Structural Characterizations. 2.2.1. Crystallography. H_3TP^+-tpy crystallizes readily as the tetrafluoroborate salt from a dichloromethane/ethyl acetate mixture to give colorless plates. The molecular structure of the ligand in $[H_3TP^+\text{-tpy}](BF_4)\cdot 0.5CH_3CO_2C_2H_5$ is given in Figure 1.

Slightly yellow colored crystals of H_3TP^+-ptpy of poor quality were obtained from ethanol/diethyl ether solution. An ORTEP drawing of the molecular structure of the ligand in $[H_3TP^+\text{-ptpy}](\text{anion})\cdot$solvent is available as Supporting Information. Due to the nondetermination of the cocrystallized molecules (counteranion and possibly solvent), we have no deposited data for this structure (see Experimental Section). Nevertheless, atomic coordinates of the organic ligand itself have been satisfactory localized, and a two-fold orientational disorder of the terminal phenyl ring could even be successfully modeled.

Single crystals of the **P0A/Ru** complex suitable for X-ray structure analysis were obtained by slow evaporation of a solution of the compound in acetonitrile. The molecular structure of the complex **P0A/Ru** within $[(tpy)Ru(tpy\text{-}TPH_3^+)](PF_6)_3\cdot 0.8CH_3CN\cdot 0.5H_2O$ is depicted in Figure 2.

Single crystals of $[Ru(ptpy\text{-}TPH_3^+)_2](PF_6)_4$ suitable for X-ray structure analysis were obtained by slow vapor diffusion of diethyl ether into an acetonitrile solution of the complex. The molecular structure of the complex **P1A$_2$/Ru** is given in Figure 3. The length of this rigid rod-like complex is 34.4 Å edge-to-edge (terminal hydrogen atoms not included). The distance, d_{MN}, between the metal center of P1 and the $N_{pyridinio}$ atoms of the acceptor moieties (A), was determined as 10.4 Å.

Classical features, regarding the 2,2′:6′,2″-terpyridyl chelating part (tpy) of the ligands, are the changing conformations of the pyridines with respect to their interannular C−C bonds observed on passing from the free ligand (anti−anti, i.e., transoid conformation) to the complexed form.[32] Indeed, for chelating purposes, the two terpyridyl fragments that participate in the inorganic core within the P0- and P1-based complexes have adopted a syn−syn (i.e., cisoid) conformation. These two ligands are mutually arranged about each metal center in an almost orthogonal fashion. The resulting local environment around the Ru^{2+} cation is therefore pseudo-octahedral (D_{2d}), with shortened Ru−N bonds (d_{Ru-N}, mean = 1.977 Å) along the main molecular axis (i.e., the bond that connects the Ru^{2+} to the central pyridine ring of each tpy ligand). The average value over **P0A/Ru** and **P1A$_2$/Ru** complexes of d_{Ru-N} when lateral pyridines of the tpy ligands are involved is 2.068 Å.

An important structural feature of these triphenylpyridinio-derivatized molecules (ligands and complexes), that actually motivates the present crystallographic study, is related to the local topology about the acceptor moiety, which has to do with the electronic communication between P and A subunits. More precisely, the conformations adopted by bulky aryl groups situated on either side of the pyridinio nitrogen atom, as well as that of the aromatic *N*-group Ar^1 (Figures 2 and 3), are under investigation. Significant geometrical data collected out of this work and retrieved from the Cambridge Structural Database,[33] for 1,2,4,6-tetraarylpyridinium and related molecules (Figure 4), are gathered in Table 1.

(31) Constable, E. C.; Cargill Thompson, A. M. W.; Tocher, D. A.; Daniels, M. A. M. *New J. Chem.* **1992**, *16*, 855−867.

(32) Thummel, R. P.; Jahng, Y. *Inorg. Chem.* **1986**, *25*, 2527−2534.

(33) Allen, F. H.; Davies, J. E.; Johnson, O. J.; Kennard, O.; Macrae, C. F.; Mitchell, E. M.; Mitchell, G. F.; Smith, J. M.; Watson, D. G. *J. Chem. Inf. Comput. Sci.* **1991**, *31*, 187−204.

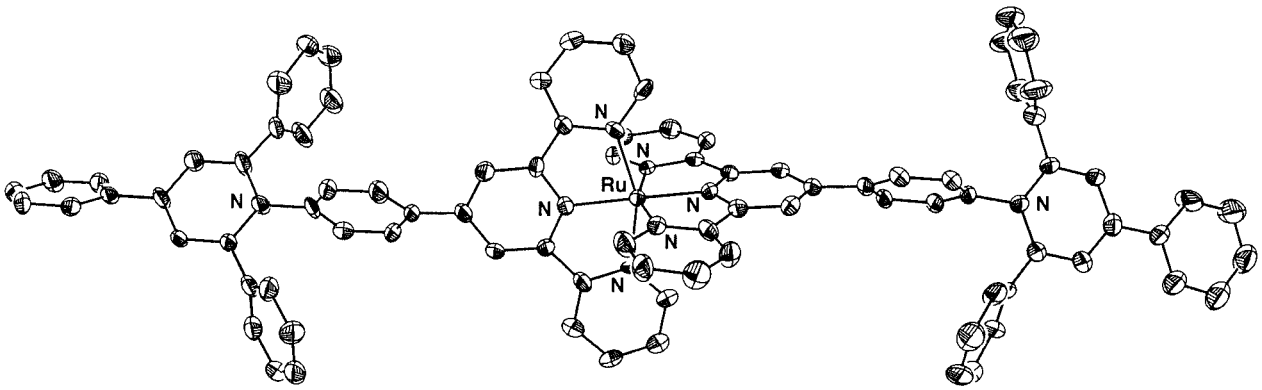

Figure 3. ORTEP drawing of the $[(H_3TP^+\text{-ptpy})Ru(ptpy\text{-}TPH_3^+)]^{4+}$ complex, **P1A$_2$/Ru**, with thermal ellipsoids (30% probability). The hydrogen atoms and PF_6^- counterions are omitted for clarity.

Table 1. Selected Bond Lengths and Dihedral Angles (θ) between the Central Pyridinium Ring and Peripheral Aryl Mean Planes

entry	Ar^1	$d(C_{Ar^1}\text{–}N_{py^+})$[g]	(θ1°)	R^2(θ2°)	R^3	R^4(θ4°)	R^5	R^6(θ6°)
H_3TP^+-tpy	py	1.4659(10)	(78.71)	H(55.92)	H	H(25.14)	H	H(71.18)
H_3TP^+-ptpy	ph	1.440(3)	(72.60)	H(62.42)	H	H(16.45)	H	H(65.11)
						H(37.03)		
P0A/Ru	py	1.439(6)	(79.38)	H(85.48)	H	H(24.29)	H	H(78.31)
P1A$_2$/Ru	ph	1.431(3)	(87.42)	H(72.85)	H	H(46.93)	H	H(87.42)
	ph	1.420(3)	(89.21)	H(65.32)	H	H(2.13)	H	H(73.81)
a	ph	1.459	(77)	H(84)	H	H(20)	H	H(72)
b	ph	1.460	(78)	H(72)	H	H(25)	H	H(59)
c	*p*-O_2SCH_2ph	1.463	(70)	H(51)	H	H(20)	H	H(50)
d	*p*-HOph	1.459	(70)	H(53)	H	H(22)	H	H(66)
e	*p*-$^-$Oph	1.479(8)	(65)	H(54)	H	*p*-Br(18)	H	H(70)
f	*p*-HOph	1.470	(73)	H(59)	O-	H(53)	H	H(47)

[a] Reference 34. [b] Reference 35. [c] Reference 36. [d] Reference 37. [e] Reference 38. [f] Reference 39. [g] Reference 40.

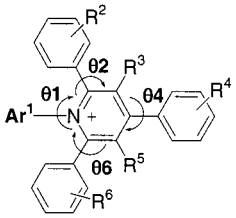

Figure 4. Parameters for Table 1.

Taking into account the overall set of data (Table 1), the main topological features may be summarized as follows. On one hand, the two aromatic substituents in ortho (i.e., 2,6-) positions of the pyridinium rings (Figure 4) are found to be tilted with respect to their supporting plane ($(\theta 2 + \theta 6)/2$, mean = 66.13°). On the other hand, these latter pyridinium rings are observed to be oriented almost perpendicularly to the plane of the Ar^1 moiety they are attached to (θ1, mean = 76.39°). These general trends are even more striking when considering the complexes only. Indeed, the average value of $(\theta 2 + \theta 6)/2$ is 77.20°, and that of the dihedral angle θ1, between the pyridinium rings and the connected coordination plane of the tpy (P0 series) or the plane of the phenyl spacer (for P1), is 85.34°. These particular conformations result from internal steric hindrance about the interannular bond that connects Ar^1 and the pyridinium part (Figures 2 and 3), i.e., between hydrogen atoms facing the $N_{pyridinio}$ atom and the two latter 2,6-aryl substituents of the pyridinium ring. In the present case, these hydrogen atoms are H(3′A) and H(9A) from the central pyridine ring of the tpy ligand (P0 series) and from the phenyl spacer (P1 series), respectively (Scheme 1). In other words, the acceptor fragment, A, is shown to be geometrically almost "decoupled" [41] from the photosensitizer, P, in the solid state because of localized *intraligand* constraints.[34]

2.2.2. NMR Study. ^{1}H and ^{13}C NMR techniques performed on diamagnetic coordination compounds gave expected results in regard to what is known in the literature for bis(phenyl)-terpyridyl transition metal complexes.[22,31,42] Where necessary, assignments were checked by performing 2D homonuclear (^{1}H−^{1}H) and heteronuclear (^{1}H−^{13}C) COSY experiments. Thus, classically, NMR signatures of heteroleptic compounds are roughly the superposition of those of the corresponding reference homoleptic complexes,[31] indicating that two tpy ligands assembled around a metal ion are structurally independent. However, this is no longer true when considering more subtle phenomena related to electronic effects, as is the shielding/deshielding of proton resonance that originates from the so-

(34) Farag, I. S. A.; El-Shora, A. I.; Rybakov, V. B. *Cryst. Res. Technol*. **1990**, *25*, 519−524.
(35) Othman, A. H.; Zakaria, Z.; Ng, S. W. *J. Crystallogr. Spectrosc. Res*. **1993**, *23*, 921.
(36) Milart, P.; Stadnicka, K. *Liebigs Ann./Recueil* **1997**, 2607−2611.
(37) Milart, P.; Mucha, D.; Stadnicka, K. *Liebigs Ann*. **1995**, 2049−2051.
(38) Allmann, R. *Z. Kristallogr*. **1969**, *128*, 115−132.
(39) Katritzky, A. R.; Ramsden, C. A.; Zakaria, Z.; Harlow, R. L.; Simonsen, S. *J. Chem. Soc., Perkin Trans. 1* **1980**, 1870−1878.
(40) Surprisingly, it is worth noting that the length, $d(C_{Ar^1}\text{−}N_{py^+})$, of the bond connecting the pyridinio nitrogen atom to its substituent (Ar^1) carbon atom (independently of whether an aryl or pyridine ring is involved, Table 1) is slightly, but sizably, diminishing as the dihedral angle θ1 gets closer to 90° ($d(C_{Ar^1}\text{−}N_{py^+})$, mean = 1.453 Å), as evidenced by the plot of $d(C_{Ar^1}\text{−}N_{py^+})$ as a function of θ1 (Supporting Information). A theoretical study has been undertaken in order to explain this not straightforwardly understandable finding, that apparently correctly models this behavior (Prof. F. Volatron, private communication).
(41) In this paper, the term "geometrical decoupling" refers to the marked twist angle (i.e., pseudo-orthogonal conformation) between the planes of two components directly linked by a single bond.
(42) Collin, J.-P.; Guillerez, S.; Sauvage, J.-P.; Barigelletti, F.; De Cola, L.; Flamigni, L.; Balzani, V. *Inorg. Chem.* **1992**, *31*, 4112−4117.

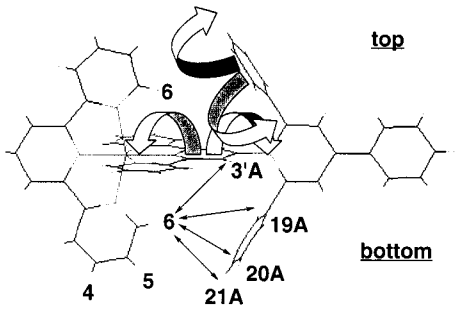

Figure 5. Pictorial representation of the ring current effects on H(6) (1D ^{1}H NMR, top) and of through-space proton−proton interaction between H(6) and the facing ligand (ROESY experiment, bottom) within **P0A/Ru** (X-ray structure).

called ring-current effects. A known example of such a through-space *interligand* interaction—for bis-terpyridyl compounds—is the pronounced shielding of H(6) (Scheme 1 and Figure 5) when complexed as compared to the related chemical shift for the free ligand. This shielding is ascribed to the proton lying over the π-cloud of the nearby central pyridine ring belonging to the other tpy ligand.[31,32] In the present work, it was found that such a through-space effect enables us to get precious structural information regarding the topology of the ligand about the acceptor fragment, i.e., concerning the actual degree of conjugation between P and A moieties. Indeed, in the case of the P0-based polyads and contrary to the P1 series of compounds, fixedly positioned H(6) protons—directly adjacent to the nitrogen atom of the external pyridines of the tpy ligand (Scheme 1 and Figure 5)—give the unique opportunity to probe the questioned planarity of the H_3TP^+-tpy ligand (see Figures 2 and 5). As a matter of fact, when comparing ^{1}H NMR spectra of **P0A/Ru** and **P0A$_2$/Ru** with the ^{1}H NMR spectrum of the reference **P0/Ru** (Figure 6), an interesting feature appears: the exceptional upfield-shifted signal of these latter H(6) protons. The reason put forward to explain such a behavior is that proton H(6) is not only surrounded by the shielding cone of the central pyridine ring of the opposite H_3TP^+-tpy ligand[31,32] but is also allowed to experience the ring current effects of the tilted phenyl ortho substituents of its 4′-attached pyridinium ring (Figure 5). The existence of the latter supplementary shielding effect ($\Delta\delta \approx -0.6$ ppm) clearly indicates that the pyridinium ring of the acceptor component is almost perpendicular to the plane of the connected tpy moiety.

Besides the reported *interligand* ring current effect, additional evidence for the "*geometrical decoupling*"[41] of P and A may be obtained from the study of the *intraligand*-related phenomenon within the same H_3TP^+-tpy series of compounds. Indeed, one may notice that (i) H(3′A) appears to be significantly shielded by −0.3 ppm with respect to H(3′) of the reference coordinated tpy (Figure 5) and (ii) a similar upfield shift is also observed when comparing resonances of H(3) and H(3A) detected at 8.47 and 8.10 ppm, respectively. These behaviors suggest, in accordance with previous conclusions, that either or both dihedral angles θ1 and θ2/θ6 (Figure 4, Table 1) slightly deviate from the strict orthogonality, allowing H(3′A) and H(3A) to experience the above-mentioned ring current effects. It is worth noting that the chemical shift of H(3′A) actually results from the balance between various contributions which are mainly the electron-withdrawing effect originating from the pyridinium (deshielding) and the ring current effect (shielding) coming from the phenyl groups adjacent to the $N_{pyridinio}$ atom, making the shielding measured for H(3′A) apparently smaller than that for H(3A).

Finally, a direct proof of the pronounced tilt between P and A is provided by NMR experiments based on the nuclear Overhauser effect (NOE), allowing the measurement of through-space couplings between protons.[43] Indeed, NOESY and ROESY (see Supporting Information) experiments carried out on **P0A/Ru** evidenced that *through-space interligand couplings do take place between the probe H(6) of the tpy ligand and protons H(21A), H(20A), and even H(19A) from the tilted phenyl substituents* adjacent to the $N_{pyridinio}$ atom of the other ligand (H_3TP^+-tpy). Furthermore, these couplings are found to be of the same order of magnitude as—and even stronger than—that of H(6) with H(3′A), which are geometrically fixed within the rigid coordination sphere at a distance ranging from 4.482 to 4.786 Å (X-ray data). Owing to the intrinsic limitation of the method that allows the detection of couplings between protons separated by a distance ranging from 2 to ca. 4.5 Å, the occurrence of these couplings is only compatible with a dihedral angle θ1 (Figure 4) between the tpy and pyridinium mean planes very close to 90°. The phenyl rings in the 2,6-positions of the pyridinium ring are then also assumed to be tilted with respect to their supporting pyridinium fragment,[44] due to an internal and local steric hindrance. Hence, one may consider that the actual conformation of **P0A/Ru** in solution is very similar to that determined in the solid state by X-ray structure analysis, confirming the "*geometrical decoupling*"[41] already asserted by Sun et al. for purely organic oligomeric analogues.[45]

2.3. Shared Structural Features and Consequences. The present work is related to strongly anisotropic molecules, showing a pronounced axial symmetry, that are expectedly suitable for directional and possibly vectorial PET. These compounds may be classified as polyad systems, as they are made of covalently linked building blocks such as electron-acceptor (A) and -donor (D) entities, which are linearly assembled on both sides of a photosensitizer (P). With the help of phenyl spacers (p) inserted between the P and D/A units, this particular arrangement allows the optimal remote location of the redox-active sites. Such a geometrical disposition actually results from the intrinsic nature of the central chromophore, which consists of two terdentate terpyridyl ligands complexed around an octahedral transition metal cation (M), Ru(II) or Os(II), in a *trans-meridional* fashion. Indeed, attachment of electroactive components at the 4′-position of both tpy ligands—in some cases via phenyl spacers—gives rise to rigid rod-like complexes that roughly have the rotation motion along their main axis as the only degree of freedom.

First, the status of phenyl spacers (p) between P and D/A, when present, deserves to be discussed. Their original role is actually dual. On one hand, it consists of locating D/A groups away from P so as to retard charge recombination and draw out CS-state lifetimes when formed (charge separation purposes) without altering the rigidity of the overall system. On the other

(43) Sanders, J. K. M.; Hunter, B. K. *Modern NMR spectroscopy*, 2nd ed; Oxford University Press: Oxford, 1993.
(44) Typically, the X-ray analysis of **P0A/Ru** gives the following distances between the probe H(6) and the through-space coupled protons of the facing acceptor ligand: 3.727 and 4.093 Å for H(6)−H(21A); 3.564, 3.895, 4.439, and 5.024 Å for H(6)−H(20A); 4.210, 4.746, 5.186, and 5.638 Å for H(6)−H(19A).
(45) Sun, X.; Yang, Y.-K.; Lu, F. *Macromolecules* **1998**, *31*, 4291−4296.

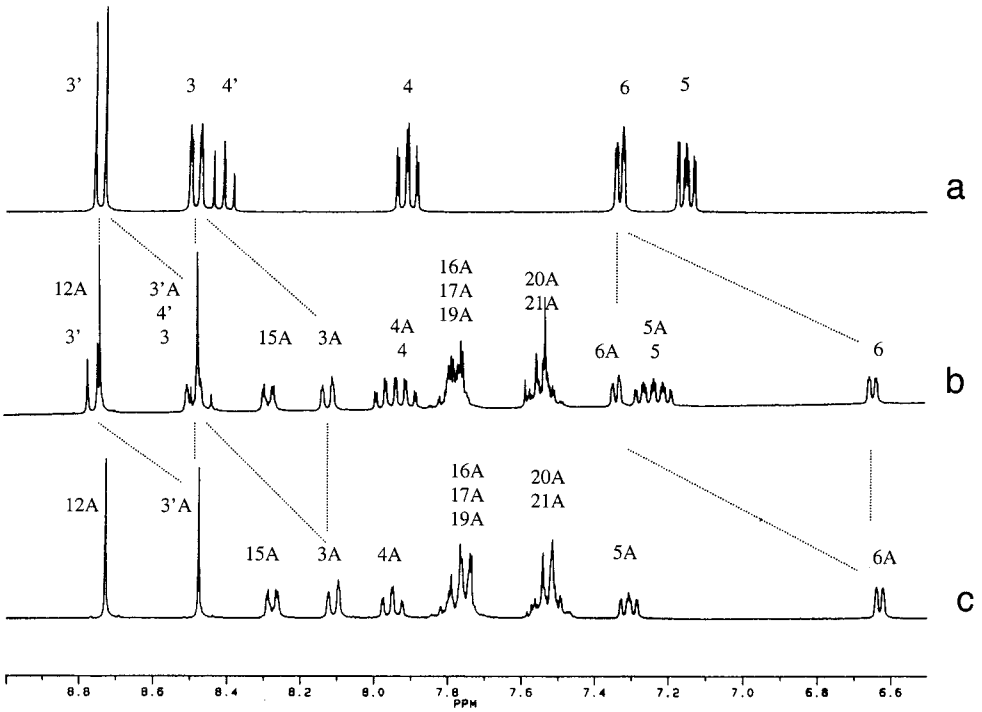

Figure 6. ^{1}H NMR spectra of CD_3CN solutions of **P0/Ru** (a), **P0A/Ru** (b), and **P0A$_2$/Ru** (c).

hand, it contributes to the improvement of the photophysical properties of the M(II)-bisterpyridyl chromophoric core (P). Indeed, the dihedral angle (θ) between this latter phenyl moiety and the central pyridine ring of the tpy ligand is rather small (θ, mean = 24.81°, range = 2.47−43.30°).[46] This allows an extension of the conjugation and thus an electronic delocalization over the entire phenyl-terpy (ptpy) skeleton.[5,22] Therefore, these issues legitimate (i) the distinction we have made between the various polyad systems depending on the absence, P0, or the presence, P1, of phenyl spacers (i.e., P1 rather than p-P0-p, see Chart 2) and (ii) our choice of different related model photosensitizer for each series.

As previously emphasized, an important question to be answered within the framework of this work is *the actual degree of conjugation* of A and D with P that determines, to a large extent, the strength of the intercomponent electronic coupling. Regarding the P/A couple, the situation is tightly connected to the value of the dihedral angle (θ1)[47,48] between the acceptor pyridinium ring of H_3TP^+ and the plane of the N-group, Ar^1, that belongs to the photosensitizer P (Figure 4). What is known from X-ray analysis is that the internal steric hindrance around the $N_{pyridinio}$ atom is such that both aryl groups in 2- and 6-positions for the pyridinium ring are tilted with respect to the ring bearing them. The steric constraints about the interannular bond that connects the pyridinium ring and its N-aryl substituent (phenyl or pyridyl) is sufficient to produce the "geometrical decoupling"[41] of the components (Table 1, $\theta 1 \approx 90°$).[34,45] Moreover, this resulting steric interaction between P and A within the P0 series of complexes is not appreciably different from that within the P1 family of compounds. *Hence, conclusions drawn out of the structural study of P0 species may therefore be extrapolated to the P1 analogues.*

However, beyond these solid-state issues, it remains of crucial importance to get insights regarding the actual conformation of molecules in solution, i.e., in the real conditions for which their physical properties are investigated. This allows one to establish a possible structure vs properties correlation. For the present purposes and beyond its routine use for the structural characterization, the ^{1}H NMR technique was revealed to be very well adapted and informative. First, the local topology about the acceptor moiety within polyad compounds in solution has to be elucidated. Interestingly, in the particular case of **P0A/Ru**, protons H(6) and H(6″) from the native tpy ligand are fixedly positioned in such a manner that the direct surrounding of the $N_{pyridinio}$ atom of the acceptor moiety—attached to the opposite tpy ligand—may be directly probed by taking advantage of both ring current and the through-space Overhauser nuclear effects. Indeed, we have unambiguously shown that, in solution, the pyridinium ring of the electron acceptor center remains almost perpendicular to the plane of the supporting tpy fragment, as it is evidenced in the solid state (X-ray analysis). Thus, in accordance with our previous reasoning about the structural similarities between P0−A and P1−A, and based on other indirect NMR considerations, the "geometrical decoupling" of H_3TP^+ from P is also established for the P1 series of complexes. Moreover, notice that theoretical calculations performed for the organic analogous pyridinium *N*-phenolate dye, Betaine-30, have shown that the more stable conformation of such a molecule in

(46) Cambridge Structural Database statistical search,[33] 40 entries.
(47) (a) Fisher, H.; Tom, G. M.; Taube, H. *J. Am. Chem. Soc.* **1976**, *98*, 5512−5517. (b) Larson, S. *J. Am. Chem. Soc.* **1981**, *103*, 4034−4040. (c) Joachim, C.; Launay, J.-P. *Chem. Phys.* **1986**, *109*, 93−99. (d) Woitellier, S.; Launay, J.-P.; Joachim, C. *Chem. Phys.* **1989**, *131*, 481−488. (e) Gourdon, A. *New J. Chem.* **1992**, *16*, 953−957. (f) Dong, T.-Y.; Huang, C.-H.; Chang, C.-K.; Wen, Y.-S.; Lee, S.-L.; Chen, J.-A.; Yeh, W.-Y.; Yeh, A. *J. Am. Chem. Soc.* **1993**, *115*, 6357−6368. (g) Pierce, D. T.; Geiger, W. E. *Inorg. Chem.* **1994**, *33*, 373−381. (h) Das, A.; Maher, J. P.; McCleverty, J. A.; Navas Badiola, J. A.; Ward, M. D. *J. Chem. Soc., Dalton Trans.* **1993**, 681−686. (i) Beer, P. D.; Chen, Z.; Grieve, A.; Haggitt, J. *J. Chem. Soc., Chem. Commun.* **1994**, 2413−2414.
(48) (a) Chen, P.; Curry, M.; Meyer, T. J. *Inorg. Chem.* **1989**, *28*, 2271−2280. (b) Berg-Brennan, C.; Subramanian, P.; Absi, M.; Stern, C.; Hupp, J. T. *Inorg. Chem.* **1996**, *35*, 3719−3722. (c) Damrauer, N. H.; Boussie, T. R.; Devenney, M.; McCusker, J. K. *J. Am. Chem. Soc.* **1997**, *119*, 8253−8268. (d) Liard, D. J.; Vlcek, A., Jr. *Inorg. Chem.* **2000**, *39*, 485−490.

Table 2. Electronic Absorption Data and Assignments

	λ_{max} [nm] (ϵ [10^4 M^{-1} cm^{-1}])		
		^{1}MLCT	^{3}MLCT
P0/Ru	271 (3.87), 308 (6.42)	475.5 (1.48)	
P0A/Ru	271.5 (5.13), 309 (8.59)	488 (2.09)	
P0A$_2$/Ru	274 (5.11), 313 (9.94)	491 (2.86)	
P1/Ru	285 (7.86), 310 (8.77)	490 (3.39)	
P1A/Ru	312 (11.65)	491.5 (3.63)	
P1A$_2$/Ru	312.5 (14.64)	493 (4.13)	
DP1/Ru	232 (4.39), 286 (6.40), 309 (9.22), 382 (1.32)	499.5 (4.05)	
D$_2$P1/Ru	238.5 (4.84), 275 (5.13), 287 (5.32), 309.5 (10.53), 388 (2.95)	514 (5.46)	
DP1A/Ru	287 (7.62), 310 (11.33)	497 (4.10)	
P1/Os	286 (7.64), 314.5 (8.64)	490 (3.01)	645 (0.67), 668 (0.77)
P1A/Os	290 (7.82), 315 (11.22)	491 (3.32)	642 (0.68), 668 (0.77)
P1A$_2$/Os	315.5 (14.59)	491 (3.90)	645 (0.78), 671 (0.93)
DP1/Os	231 (4.98), 287.5 (6.47), 313 (9.90), 386 sh (2.15)	501 (4.07)	648 (0.96), 672 (1.05)
D$_2$P1/Os	238 (4.95), 276 (5.19), 313 (10.62), 349 (4.62), 380 sh (3.54)	512 (4.84)	653 (1.20), 676 (1.35)
DP1A/Os	313 (11.94)	503 (4.21)	644 (0.92), 674 (0.92)

solution in polar solvents corresponds to a value of $\theta 1$ close to 90°.[49]

Concerning the P1/D couple, when borne by an aryl group, the geometry around the N_{amino} atom of a D fragment of the 4-*N*,*N*-disubstituted amino type is known to be that of a flattened pyramid,[50] almost coplanar with the latter supporting ring with the nitrogen lone pair being delocalized over it (when no steric hindrance interferes). In other words, such electron-releasing substituents behave as conjugated aromatic amines, strongly coupled to P (P0 and P1). This is, for instance, the case for the **D$_2$P0/Ru** complex (D = NMe_2), as previously reported by Constable et al.[31]

2.4. Electronic Behaviors. Ground-state absorption spectra of all polyads and reference compounds were recorded; the corresponding data are collected in Table 2. The main features obtained are classical for Ru(II)- and Os(II)-bisterpyridyl complexes.[5] In the near-UV part of the spectra, ligand-centered (LC) transitions originating from both tpy/ptpy fragments and the organic acceptor subunit, H_3TP^+, are observed. Spin-allowed $d\pi(M^{II}) \rightarrow \pi^*(L)$ metal-to-ligand charge transfer (^{1}MLCT) transitions are detected in the visible region around 500 nm. The strong spin−orbit coupling of the Os(II) metal cation partially allows the normally spin-forbidden ^{3}MLCT transitions. These are therefore observed in the far-visible−near-IR region as poorly resolved bands of weak intensity.

Classical behaviors are also the bathochromic shift and the hyperchromic effect of the photosensitizer-centered ^{1}MLCT transition (mainly) that accompany its electronic coupling with substituents, regardless of their electron-withdrawing or -releasing nature.[5,31,51] Indeed, obvious perturbations of the chromophores are evidenced within (i) the P0/Ru-based series of complexes where the H_3TP^+ moiety is directly connected to the tpy ligand (red-shift up to ca. 15 nm associated with a molar extinction coefficient enhancement of ca. 100%) and (ii) the P1-based polyads that involve the dimethylamino electron-donor substituent (red-shift of at least 10 nm associated with an ϵ enhancement and a new band rising at ca. 380 nm). Besides, the latter finding is observed independently of whether the metal cation is Ru(II) (see Figure 7a) or Os(II).

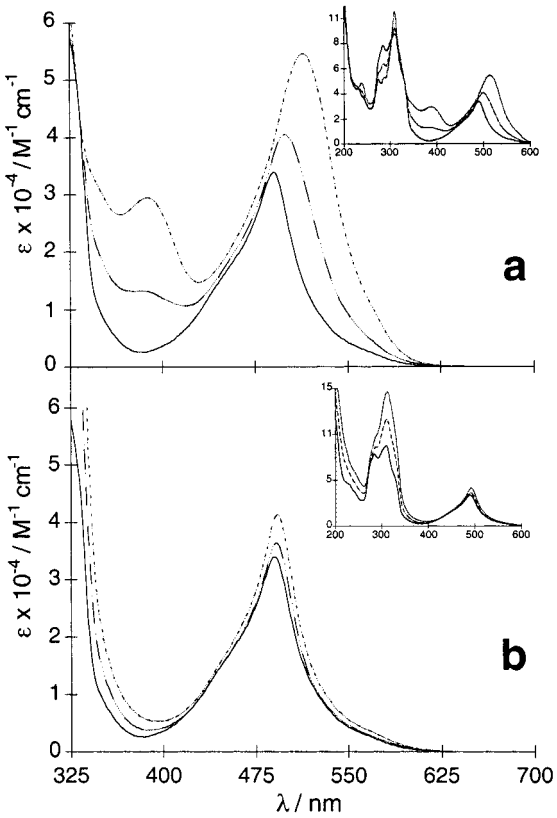

Figure 7. Absorption spectra (room temperature, acetonitrile solution). (a) **P1/Ru** (solid), **DP1/Ru** (dashed), and **D$_2$P1/Ru** (dotted). Inset: Overall representation. (b) **P1/Ru** (solid), **P1A/Ru** (dashed), and **P1A$_2$/Ru** (dotted). Inset: Overall representation.

Bathochromic shifts and hyperchromic effects that normally account for the extension of conjugation (π delocalization) and the mediation of electronic effects (electron-withdrawing or -releasing substituent effects) are both indicative of strong intercomponent electronic couplings.[5] These trends follow a progressive variation upon increasing the number of electron-donating or -withdrawing substituents, i.e., on passing from dyads (DP1 and P0A heteroleptic compounds) to reference triads (D_2P1 and $P0A_2$ homoleptic species). Such behaviors have been rationalized by Maestri et al.[51] in terms of differential acceptor-induced stabilization and donor-induced destabilization of the frontier HOMO (π_M) and LUMO (π^*_L) orbitals.

A careful analysis of the electronic properties of the ptpy-

(49) (a) Mente, S. R.; Maroncelli, M. *J. Phys. Chem. B* **1999**, *103*, 7704−7719. (b) Bartkowiak, W.; Lipinski, J. *J. Phys. Chem. A* **1998**, *102*, 5236−5240.
(50) Gourdon, A.; Launay, J.-P.; Bujoli-Doeuff, M.; Heisel, F.; Miehé, J. A.; Amouyal, E.; Boillot, M.-L. *J. Photochem. Photobiol. A: Chem.* **1993**, *71*, 13−25.
(51) Maestri, M.; Armaroli, N.; Balzani, V.; Constable, E. C.; Cargill Thompson, A. M. W. *Inorg. Chem.* **1995**, *34*, 2759−2767.

Table 3. Summary of Crystallographic Data for $[H_3TP^+$-tpy$](BF_4)\cdot 0.5CH_3CO_2C_2H_5$, $[H_3TP^+$-ptpy$]$(Anion)·Solvent, $[(tpy)Ru(tpy\text{-}TPH_3^+)](PF_6)_3\cdot 0.8CH_3CN\cdot 0.5H_2O$, and $[Ru(ptpy\text{-}TPH_3^+)_2](PF_6)_4$

compound	$[H_3TP^+$-tpy$](BF_4)\cdot 0.5CH_3CO_2C_2H_5$	$[H_3TP^+$-ptpy$]$(anion)·solvent	P0A/Ru·0.8CH$_3$CN·0.5H$_2$O	P1A$_2$/Ru
empirical formula	$C_{38}H_{27}N_4\cdot BF_4\cdot CH_3CO_2C_2H_5$	$C_{44}H_{31}N_4\cdot$Cl/anion·solvent	$C_{53}H_{38}N_7Ru\cdot 3PF_6\cdot 0.8CH_3CN\cdot 0.5H_2O$	$C_{88}H_{62}N_8Ru\cdot 4PF_6$
formula weight	714.550	615.728·Cl/anion·solvent	1350.735	1912.406
T, K	293(2)	293(2)	293(2)	293(2)
wavelength, Å	1.54178	1.54178	0.71073	0.71073
crystal system	triclinic	monoclinic	triclinic	orthorhombic
space group	$P\bar{1}$	$P2_1/c$	$P\bar{1}$	*Pbca*
color	colorless	pale yellow	orange	orange-red
crystal size, mm	0.34 × 0.32 × 0.24	0.35 × 0.12 × 0.10	0.32 × 0.15 × 0.05	0.30 × 0.09 × 0.03
a, Å	10.446(2)	13.469(2)	14.366(3)	16.355(3)
b, Å	13.750(2)	9.530(2)	14.570(3)	16.690(3)
c, Å	14.169(4)	30.088(3)	14.677(3)	60.729(12)
α, deg	116.59(3)	90	82.82(3)	90
β, deg	105.55(3)	94.16(3)	75.68(3)	90
γ, deg	93.46(3)	90	82.19(3)	90
V, Å^3	1714.4(6)	3851.8(11)	2935.6(10)	16577(6)
Z	2	4	2	8
ρ_{calc}, g cm^{-3}	1.303	1.196	1.524	1.533
μ, mm^{-1}	0.780	1.196	0.451	0.373
F(000)	694	1435	1350	7728
θ range, deg	3.68−66.94	2.95−45.65	2.47−22.49	1.39−20.96
limiting indices	$-12 \le h \le 12$, $-16 \le k \le 14$, $0 \le l \le 16$	$0 \le h \le 12$, $0 \le k \le 8$, $-27 \le l \le 27$	$-18 \le h \le 19$, $-19 \le k \le 18$, $-19 \le l \le 19$	$-16 \le h \le 16$, $-16 \le k \le 16$, $-60 \le l \le 60$
reflns collected	6370	3407	18 176	64 871
independent reflns	6103 [R(int) = 0.0239]	3221 [R(int) = 0.1165]	7203 [R(int) = 0.0864]	8774 [R(int) = 0.2628]
refinement method	full-matrix least-squares on F^2			
data/restraints/params	4953/0/458	2068/1760/449	6722/534/775	7386/6094/1127
goodness-of-fit on F^2	1.784	1.452	1.165	1.641
final R indices [$I > 2\sigma(I)$]	R1 = 0.0599, wR2 = 0.2037	R1 = 0.1405, wR2 = 0.3574	R1 = 0.0618, wR2 = 0.1385	R1 = 0.1304, wR2 = 0.2745
R indices (all data)	R1 = 0.0965, wR2 = 0.2382	R1 = 0.3725, wR2 = 0.5534	R1 = 0.0915, wR2 = 0.1504	R1 = 0.2087, wR2 = 0.3480
peak/hole (e·Å^{-3})	0.451/−0.232	0.503/ −0.479	0.776/−0.340	3.435/ −0.711

based chromophores (P1) shows that, in the case of polyad systems made of P1 and H_3TP^+ components only (and contrary to the P1/D family), the influence of the triphenylpyridinio moiety upon the MLCT absorption transitions is barely detected, except for a slight hyperchromic effect, as exemplified in Figure 7b. In light of the previous reasoning, this behavior is then considered as indicative of an extremely moderate intercomponent coupling.[52]

3. Summary

In this work, the first elements of a novel family of triarylpyridinio-derivatized terpyridyl ligands, i.e., H_3TP^+-tpy and H_3TP^+-ptpy have been synthesized and fully characterized. When complexed with ruthenium(II) and osmium(II) transition metal cations, nanometer-scale rigid rod-like supermolecules with a unique axis and variable length (up to ca. 34.5 Å) have been obtained. Moreover, it has been shown that, due to their particular nature as chromophoric entities and their differential electronic sensitivity toward covalently linked redox-active units, P0 and P1 are actually distinct photosensitizers.

Combined X-ray structural analysis and NMR studies have demonstrated that the rotation motion is not completely free along the main molecular axis, even in solution. Indeed, a pronounced twist angle between the photosensitizer and the pyridinium ring of the acceptor has been evidenced, originating from internal steric hindrance. As a result, concerning the P0 and P1 series of compounds, A (contrary to D) is not conjugated with the photosensitizer. However, a substituent effect (electron-withdrawing) exists in the case of the direct attachment of A to the tpy ligand (P0 series, H_3TP^+-tpy family of ligand) as well as for D-substituted P1 luminophores (electron-releasing effect). Based on these findings, *the intercomponent coupling* within the polyad systems, as a key parameter accounting for the interesting photophysical behaviors, will be discussed in further detail in a forthcoming paper. [52]

4. Experimental Section

4.1. General Experimental Details. Electronic spectra were recorded on a Perkin-Elmer Lambda 9 spectrophotometer. The CI and ES (solvent, acetonitrile) mass spectra were recorded with a modified Nermag R10-10 quadrupole mass spectrometer.

4.2. Crystal Structure Determinations. Crystal data and data collection and refinement parameters for $[H_3TP^+$-tpy$](BF_4)\cdot 0.5CH_3CO_2C_2H_5$, $[H_3TP^+$-ptpy$]$(anion)·solvent, $[(tpy)Ru(tpy\text{-}TPH_3^+)](PF_6)_3\cdot 0.8CH_3CN\cdot 0.5H_2O$, and $[Ru(ptpy\text{-}TPH_3^+)_2](PF_6)_4$ are summarized in Table 3.

4.2.1. Organic Ligands. A single crystal of each species was mounted on an automated Enraf-Nonius CAD4 diffractometer.[53] The unit cells were determined on the basis of 25 indexed and centered reflections. Intensities were collected at room temperature with the use of graphite-monochromated Cu Kα radiation (1.54178 Å) in $\omega/2\theta$ scan mode. The data were corrected for Lorentz and polarization effects, without being corrected for absorption. The intensities of three reflections were monitored during the data collection and showed no

(52) Lainé, P.; Bedioui, F.; Amouyal, E.; Albin, V.; Berruyer-Penaud, F. Submitted.

(53) Frenz, B. A. The Enraf-Nonius CAD4-SDP. In *Computing in Crystallography*; Shenk, H., Olthof-Hazenkamp, R., Van Koningveld, H., Bassi, G. C., Eds.; Delftse Universitaire Pers: Delft, The Netherlands, 1978; pp 64−71.

systematic variation throughout. The structures were solved by direct methods (SIR92)[54] and refined on F^2 with the help of SHELX93.[55]

Structure of $[H_3TP^+$-tpy$](BF_4)\cdot 0.5CH_3CO_2C_2H_5$. One cationic molecule associated with a counteranion (BF_4^-) is present in the asymmetric unit of the triclinic space group. Localization of the nitrogen atoms showed a transoid conformation for the three pyridine rings about the interannular C−C bonds, as least-squares calculations considering a cisoid conformation led to clearly poorer values of the agreement factors (wR2 = 0.270). Hydrogen atoms were geometrically positioned, except for the two hydrogen atoms attached to the ortho carbons belonging to the lateral pyridine moieties, found on Fourier difference maps. All hydrogen atoms were constrained with a riding model during refinements; all non-hydrogen atoms were refined anisotropically. A solvent region was found by Fourier synthesis, which should correspond to an ethyl acetate molecule. This solvent molecule, which contains one atom located on an inversion center, is disordered in a manner that could not be readily resolved. All attempts to constrain interatomic distances to expected values were unsuccessful. The final model is the best fit to residual density. The two maxima of residual electronic density (0.45 and 0.32 e/Å^3, respectively) were found in the solvent region.

Structure of $[H_3TP^+$-ptpy](Anion)·Solvent. Only aggregates of poorly shaped crystals could be grown. As a consequence, the structure is of rather poor quality. The asymmetric unit contains one monocationic ligand molecule and a severely disordered region. Owing to the lack of observed data, restraints for planarity and similarity of geometry and of displacement parameters were applied to the ligand. A two-fold orientational disorder of the terminal phenyl was resolved, and populations were refined to a ratio of 60/40. Least-squares refinements only suggest the expected transoid conformation of the terpyridine (found in the previous structure), which was therefore imposed to the model. Hydrogen atoms were geometrically positioned; no hydrogen was generated for the disordered phenyl. All non-hydrogen atoms were refined anisotropically, except for the carbon atoms belonging to the terminal phenyl, which were refined isotropically. The disordered region consists of a strong isolated peak, which was—arbitrarily—best assigned as a chemically not relevant chloride anion (A), and a region of residual electronic density resembling a diethyl ether molecule. Examination of X-ray diffraction patterns recorded with a STOE IPDS imaging plate system[56] (see below) led us to conclude that the assignment of the space group of $[H_3TP^+$-ptpy](anion) is problematic. Two triclinic twin domains were evidenced, these domains being twinned along the monoclinic axis. The triclinic cell parameters are very similar to the monoclinic one: $a = 13.412(3)$ Å, $b = 9.214(2)$ Å, $c = 30.269(5)$ Å; $\alpha = 92.28(3)°$, $\beta = 95.25(3)°$, $\gamma = 92.93(3)°$. A full sphere of data was collected on the image plate, and a unique set of data could be extracted and reduced in the triclinic symmetry. Investigations on the crystal structure were performed either by direct methods or by molecular replacement, but no solution was found. Attempts to refine, in the triclinic symmetry, the structural model previously obtained from the—twinned—monoclinic set of data also failed. The structure could be again solved in the monoclinic space group by using the overall twinned data from the image plate, but it was not possible to further explain the unresolved electronic density. For these reasons, we have not deposited the coordinates for this structure.

4.2.2. Inorganic Compounds. A single crystal of each species was mounted on a STOE IPDS.[56] Intensities were collected at room temperature with the use of graphite-monochromated Mo Kα radiation (0.71073 Å). The structures were solved by direct methods and refined on F^2 with the SHELXTL V5.03 package. The data were corrected for Lorentz and polarization effects as well as for absorption.

Structure of $[(tpy)Ru(tpy\text{-}TPH_3^+)](PF_6)_3\cdot 0.8CH_3CN\cdot 0.5H_2O$. The asymmetric unit is made up of one tricationic heteroleptic complex, three hexafluorophosphate anions, and one acetonitrile plus one water solvent molecules. The ruthenium(II) cation exhibits a pseudo-octahedral environment. The two terdentate ligands complexing the metal center display the expected cisoid conformation about the interannular C−C bonds. All non-hydrogen atoms were refined anisotropically. Hydrogen atoms were geometrically positioned; no hydrogen atom was generated for the solvents. The populations of the acetonitrile solvent and of the water molecule were refined to values of 0.80 and 0.50, respectively. Similarity restraints were applied to the ligands; acetonitrile bond distances/lengths were also restrained to the standard target values. The maximum of residual electronic density (0.78 e/Å^3) is located close (ca. 1 Å) to the ruthenium coordinates.

Structure of $[Ru(ptpy\text{-}TPH_3^+)_2](PF_6)_4$. Only tiny needles could be grown, and the resulting lack of observed data leads to a rather poor internal R value. The asymmetric unit is made up of one tetracationic homoleptic complex associated with four hexafluorophosphate anions. Two terpyridyl fragments achieve the completion of the coordination of the metal center, each adopting a cisoid conformation about its interannular C−C bonds. The resulting local symmetry about the Ru^{2+} cation is that of a distorted octahedron. All non-hydrogen atoms were refined anisotropically, hydrogen atoms were geometrically positioned, and a riding model was used. Restraints for planarity and similarity of geometry and of displacement parameters were applied to the two ligands. Geometrical and displacement parameter restraints were also applied to the hexafluorophosphate moieties. Final difference Fourier synthesis shows an unexpectedly high residual electronic density (3.43 e/Å^3) close (ca. 1.35 Å) to the Ru atom. Improvements of the data reduction were tried by checking the significance of integration parameters (profile function, effective mosaic spread, and pixel-overlapping tolerance). Moreover, refinements were performed in lower crystal class (*mm*2), and the monoclinic symmetry was also considered. None of the trials resulted in the elimination or the intensity weakening of this spurious peak. Thus, it may be concluded that this feature is due to the crystal specimen; i.e., a minor twin component is probably attached to the major one. The small angular deviation between the two crystal components precludes the collection of proper Bragg's peaks, especially along the very dense reciprocal direction c^* (c = 60.73 Å). Notice that the second maximum of residual electronic density stands in the expected range (0.78 e/Å^3).

4.3. NMR Experiments. Routine ^{1}H and ^{13}C NMR spectra were recorded on a Bruker AC-300 (300 MHz) spectrometer. Chemical shifts are reported in parts per million (ppm) downfield from tetramethylsilane (TMS) with reference to internal solvent. Multiplicities are abbreviated as follows: singlet (s), doublet (d), triplet (t), and multiplet (m). Unless otherwise specified (i.e., labels A and D refer to the acceptor and donor ligands, respectively), ^{1}H and ^{13}C NMR assignments refer to the tpy (P0 series) or Me-ptpy (P1 family) terminal ligands. NOESY and ROESY experiments were performed with a Bruker DMX 500 (500 MHz) spectrometer on a concentrated and deoxygenated (argon bubbling) CD_3CN solution of $[(tpy)Ru(tpy\text{-}TPH_3^+)](PF_6)_3$. NOESY experiments gave expected features for a medium-size molecule (M_r = 1308.88 g mol^{-1}), i.e., slightly positive NOE signals at 300 MHz that vanish when measured with the 500 MHz spectrometer. The ROESY spectrum of **P0A/Ru** was recorded with a mixing period τ_m = 400 ms and a strong off-resonance spin-lock (8400 Hz) pulse using an adiabatic rotation angle of 54.7°.[57]

4.4. Syntheses. Chemicals. High-purity commercial reagent grade products were used without further purification. The ligand **Me-ptpy**[22] and the complexes **(tpy)RuCl$_3$**,[31,58b] **(Me-ptpy)RuCl$_3$**,[22,58] **(Me-ptpy)-**

(54) Altomare, A.; Cascarano, G.; Giacovazzo, C.; Guagliardi, A.; Burla, M. C.; Polidori, G.; Cavalli, A. *J. Appl Crystallogr.* **1994**, *27*, 435−436.
(55) Sheldrick, G. M. *SHELXTL-Plus*, Rel. 5.03; Siemens Analytical X-ray Instruments Inc.: Madison, WI, 1995.
(56) STOE IPDS, STOE &CIE GmbH, 1997.
(57) Desvaux, H.; Berthault, P.; Birlirakis, N.; Goldman, M.; Piotto, M. *J. Magn. Reson. A* **1995**, *113*, 47−52.
(58) (a) Collin, J.-P.; Guillerez, S.; Sauvage, J.-P. *J. Chem. Soc., Chem. Commun.* **1989**, 776−778. (b) Sullivan, B. P.; Calvert, J. M.; Meyer, T. J. *Inorg. Chem.* **1980**, *19*, 1404−1407.

$OsCl_3$,[58a] **$[Ru(tpy)_2](PF_6)_2$**,[31] **$[Ru(ptpy\text{-}Me)_2](PF_6)_2$**,[22,58a] and **$[Os(ptpy\text{-}Me)_2](PF_6)_2$** [58a] were synthesized following the literature methods. Concerning all synthesized inorganic compounds, ^{1}H and ^{13}C NMR data along with full assignments are available as Supporting Information.

4′-(*p*-*N*,*N*-Dimethylaminophenyl)-2,2′:6′,2″-terpyridine, (Me_2N-ptpy). The procedure was derived from that of Collin et al. for Me-ptpy,[22] using the conveniently substituted aldehyde reactant, i.e., *p*-*N*,*N*-dimethylaminobenzaldehyde. The black gummy solid obtained was collected by decantation, thoroughly washed with H_2O, and dissolved in CH_2Cl_2 instead of being treated with HBr. The organic phase was washed several times with H_2O until the aqueous phase was colorless and neutral. After evaporation of the solvent, the solid was redissolved in a CH_2Cl_2:EtOH mixture (1:1, 500 mL), and an aqueous solution of Fe^{2+} (Mohr salt, 10 g in 100 mL of H_2O) was added to give immediately a dark purple medium, which was vigorously stirred for an additional 0.25 h. The phase separation of the reaction medium was then completed by addition of CH_2Cl_2 (200 mL) and H_2O (200 mL). The purple aqueous phase was washed several times with CH_2Cl_2 until the organic phase was colorless. Afterward, the classical method of purification[24] (anion metathesis and precipitation of the complex followed by the decomplexation step) was performed (yield: 14%). ^{1}H NMR (300 MHz, $CDCl_3$, ppm): δ 8.74 (dd, 2H, J = 4.8, 1.6 Hz; H^{6D}); 8.72 (s, 2H; $H^{3'D}$); 8.67 (d, 2H, J = 7.8 Hz; H^{3D}); 7.88 (d, 2H, J = 8.7 Hz; H^{8D}); 7.87 (dd, 2H, J = 7.0, 1.8 Hz; H^{4D}); 7.34 (ddd, 2H, J = 7.7, 4.8, 1.2 Hz; H^{5D}); 6.82 (d, 2H, J = 8.9 Hz; H^{9D}); 3.02 (s, 6H; $H^{Me/D}$). ^{13}C NMR: δ 156.92 ($C^{2'D}$); 155.92 (C^{2D}); 151.34 (C^{10D}); 150.24 ($C^{4'D}$); 149.31 (C^{6D}); 137.03 (C^{4D}); 128.30 (C^{8D}); 125.75 (C^{7D}); 123.85 (C^{5D}); 121.60 (C^{3D}); 117.75 ($C^{3'D}$); 112.51 (C^{9D}); 40.59 ($C^{Me/D}$). UV−vis (CH_3CN) λ_{max}/nm (ϵ/M^{-1} cm^{-1}): 234 (23 120), 290 (22 990), 346 (19 830). Anal. Calcd for $C_{23}H_{20}N_4$: C, 78.38; H, 5.72; N, 15.90. Found: C, 78.38; H, 5.65; N, 15.75.

4′-(*p*-Nitrophenyl)-2,2′:6′,2″-terpyridine, (O_2N-ptpy). The ligand was made by following a modification of the literature method for the synthesis of Me-ptpy,[22] using the conveniently substituted aldehyde reactant, i.e., *p*-nitrobenzaldehyde, except that no bromhydrate was precipitated. As described above for the Me_2N-ptpy ligand, the ligand was directly extracted with iron(II) as its homoleptic complex $[Fe(ptpy\text{-}NO_2)_2]^{2+}$ and purified. The final recrystallization of the O_2N-ptpy ligand was carried out in a mixture EtOH/H_2O, affording the pure product as beige needles (yield: 11%). ^{1}H NMR (300 MHz, $CDCl_3$, ppm): δ 8.76 (s, 2H; $H^{3'}$); 8.73 (dd, 2H, J = 4.8, 1.6 Hz; H^6); 8.68 (d, 2H, J = 7.9 Hz; H^3); 8.35 (d, 2H, J = 8.8 Hz; H^9); 8.04 (d, 2H, J = 8.8 Hz; H^8); 7.91 (dd, 2H, J = 7.8, 7.7 Hz; H^4); 7.39 (dd, 2H, J = 7.4, 4.8 Hz; H^5). ^{13}C NMR: δ 156.92 ($C^{2'D}$); 155.92 (C^{2D}); 151.34 (C^{10D}); 150.24 ($C^{4'D}$); 149.18 (C^6); 137.04 (C^4); 128.28 (C^8); 125.75 (C^{7D}); 124.19 (C^5); 121.41 (C^3); 117.75 ($C^{3'D}$); 118.92 (C^9). UV−vis (CH_2Cl_2) λ_{max}/nm (ϵ/M^{-1} cm^{-1}): 245 (29 970), 252 (29 460), 286 (43 220). Anal. Calcd for $C_{21}H_{14}N_4O_2 \cdot H_2O$: C, 67.73; H, 4.33; N, 15.05. Found: C, 67.67; H, 4.33; N, 15.29.

4′-(*p*-Aminophenyl)-2,2′:6′,2″-terpyridine, (H_2N-ptpy). To a solution of O_2N-ptpy monohydrate (0.5 g, 1.34 mmol) in EtOH (100 mL) was added Pd/C 10% (0.15 g), and the suspension was heated to reflux for 1 h under Ar. Hydrazine hydrate solution (N_2H_4 55%, 1.6 mL, 28.2 mmol, 21 equiv) was then added dropwise using a syringe and the reflux carried on for an additional 0.5 h. The reaction mixture was cooled to room temperature and filtered over cotton-wool, and the catalyst was washed with CH_2Cl_2 (150 mL). The combined organic filtrates were washed several times with H_2O (5 × 100 mL) until the aqueous phase was almost neutral. The organic phase was then dried over magnesium sulfate and filtered, and the solvent was evaporated, affording a pale yellow microcrystalline product (0.426 g; yield 97.7%). ^{1}H NMR (300 MHz, $CDCl_3$, ppm): δ 8.72 (dd, 2H, J = 4.8, 1.6 Hz; H^6); 8.68 (s, 2H; $H^{3'}$); 8.65 (d, 2H, J = 7.9 Hz; H^3); 7.87 (dd, 2H, J = 7.8, 7.7 Hz; H^4); 7.78 (d, 2H, J = 8.6 Hz; H^8); 7.33 (dd, 2H, J = 7.4, 4.7 Hz; H^5); 6.79 (d, 2H, J = 8.6 Hz; H^9). ^{13}C NMR: δ 156.33 ($C^{2'}$); 155.52 (C^2); 149.83 (C^{10}); 148.89 (C^6); 147.37 ($C^{4'}$); 136.69 (C^4); 128.22 (C^8); 128.00 (C^7); 123.53 (C^5); 121.20 (C^3); 117.62 ($C^{3'}$); 115.05 (C^9). These data are in agreement with those reported in the literature.[21]

1,2,4,6-Tetraphenylpyridinium, [H_3TP^+-p](0.5HSO_4, 0.5OAc). A mixture of aniline (0.25 g, 2.68 mmol), 2,4,6-triphenylpyrylium hydrogen sulfate (1.636 g, 4.026 mmol, 1.5 equiv), and anhydrous sodium acetate (1 g) in EtOH (25 mL) was heated overnight under reflux. Once the reaction medium was cooled to room temperature, the solvent was removed and the product extracted with CH_2Cl_2. The compound was subsequently purified by column chromatography over basic alumina with a gradient mixture of eluent varying from pure EtOAc to pure CH_2Cl_2. The pure product was obtained as white crystals after recrystallization from a mixture of EtOAc and CH_2Cl_2 (0.55 g; yield 44.4%). ^{1}H NMR (300 MHz, $CDCl_3$, ppm): δ 8.39 (s, 2H; H^{12A}); 8.12 (dd, 2H, J = 8.0, 1.3 Hz; H^{15A}); 7.67 (m, 3H; H^{16A}, H^{17A}); 7.43 (m, 4H; H^{19A}); 7.35 (m, 8H; H^{9A}, H^{20A}, H^{21A}); 7.19 (m, 3H; H^{7A}, H^{8A}). ^{13}C NMR: δ 152.41 (C^{11A}); 152.25 (C^{13A}); 134.59 (C^{18A}); 129.64 (C^{14A}); 128.50 (C^{17A}); 127.98 (C^{10A}); 125.79 (C^{21A}); 125.52 (C^{19A}); 125.35 (C^{8A}, C^{16A}); 124.49 (C^{12A}); 124.34 (C^{9A}); 124.0 (C^{15A}, C^{20A}); 121.57 (C^{7A}). UV−vis (CH_3CN) λ_{max}/nm (ϵ/M^{-1} cm^{-1}): 237sh (32 620), 308 (33 190). Anal. Calcd for $C_{29}H_{22}N_1(0.5HSO_4^-, 0.5CH_3CO_2^-)$: C, 77.89; H, 5.23; N, 3.03. Found: C, 77.79; H, 5.34; N, 3.00.

4′-*N*-(2,4,6-Triphenylpyridinio)-2,2′:6′,2″-terpyridine, [H_3TP^+-tpy](BF_4). A mixture of H_2N-tpy (0.372 g, 1.498 mmol), 2,4,6-triphenylpyrylium tetrafluoroborate (0.89 g, 2.247 mmol, 1.5 equiv), and anhydrous sodium acetate (1.2 g) in EtOH (30 mL) was refluxed 14 h. After evaporation of the solvent in a Rotavapor, the product was extracted from the solid with CH_2Cl_2 and purified by column chromatography over basic alumina using a mixture of eluents with an increasing gradient of polarity. The elution was performed with EtOAc/CH_2Cl_2, 100:0 to 0:100, and then with CH_2Cl_2/EtOH, 99:1 to 50:50. After recrystallization from a mixture CH_2Cl_2/EtOAc, the pure product was obtained as colorless prismatic crystals (0.659 g; yield 65.6%). ^{1}H NMR (300 MHz, $CDCl_3$, ppm): δ 8.61 (d, 2H, J = 4.7 Hz; H^{6A}); 8.36 (s, 2H; $H^{3'A}$); 8.35 (d, 2H, J = 7.9 Hz; H^{3A}); 8.11 (s, 2H; H^{12A}); 7.89 (dd, 2H, J = 8.1, 1.3 Hz; H^{15A}); 7.78 (ddd, 2H, J = 7.8, 7.7, 1.6 Hz; H^{4A}); 7.57 (m, 4H; H^{19A}); 7.51 (m, 3H; H^{16A}, H^{17A}); 7.29 (dd, 2H, J = 7.5, 4.8 Hz; H^{5A}); 7.22 (m, 6H; H^{20A}, H^{21A}). ^{13}C NMR: δ 158.73 (C^{13A}); 157.47 ($C^{2'A}$); 156.37 (C^{2A}); 153.94 (C^{11A}); 149.80 (C^{6A}); 148.51 ($C^{4'A}$); 137.18 (C^{4A}); 134.69 (C^{14A}); 132.55 (C^{18A}); 132.46 (C^{17A}); 130.81 (C^{21A}); 130.00 (C^{16A}, C^{19A}); 128.93 (C^{15A}, C^{20A}); 126.76 (C^{12A}); 124.92 (C^{5A}); 121.59 (C^{3A}); 120.21 ($C^{3'A}$). UV−vis (CH_3CN) λ_{max}/nm (ϵ/M^{-1} cm^{-1}): 308 (50 800). Anal. Calcd for $C_{38}H_{27}N_4BF_4 \cdot 0.5CH_3CO_2C_2H_5$: C, 71.65; H, 4.66; N, 8.35. Found: C, 71.19; H, 4.44; N, 8.14.

4′-[4-*N*-(2,4,6-Triphenylpyridinio)phenyl]-2,2′:6′,2″-terpyridine, [H_3TP^+-ptpy](0.1HSO_4, 0.9OAc). The procedure was similar to that described for H_3TP^+-tpy, using H_2N-ptpy (0.426 g, 1.313 mmol), 2,4,6-triphenylpyrylium hydrogen sulfate (0.8 g, 1.97 mmol, 1.5 equiv), and anhydrous sodium acetate (1.0 g) in EtOH (25 mL) heated to reflux for 20 h. The final recrystallization was performed in pure Et_2O, leading to yellowish-ochre aggregated crystals (0.665 g; yield 74.6%). ^{1}H NMR (300 MHz, $CDCl_3$, ppm): δ 8.65 (d, 2H, J = 4.8 Hz; H^{6A}); 8.57 (d, 2H, J = 7.9 Hz; H^{3A}); 8.46 (s, 2H; $H^{3'A}$); 8.15 (s, 2H; H^{12A}); 7.94 (d, 2H, J = 8.0 Hz; H^{15A}); 7.83 (dd, 2H, J = 7.9, 7.6 Hz; H^{4A}); 7.75 (d, 2H, J = 8.7 Hz; H^{8A}); 7.62 (m, 4H; H^{19A}); 7.59 (d, 2H, J = 8.7 Hz; H^{9A}); 7.54 (m, 3H; H^{16A}, H^{17A}); 7.33 (dd, 2H, J = 4.8 Hz; H^{5A}); 7.29 (m, 6H; H^{20A}, H^{21A}). ^{13}C NMR: δ 156.73 ($C^{2'A}$); 156.58 (C^{13A}); 155.82 (C^{2A}); 155.46 (C^{11A}); 148.85 (C^{6A}); 147.74 ($C^{4'A}$); 139.59 and 139.50 (C^{7A}, C^{10A}); 136.91 (C^{4A}); 133.90 (C^{14A}); 132.70 (C^{18A}); 132.20 (C^{17A}); 130.24 (C^{21A}); 129.75 (C^{19A}); 129.58 (C^{16A}); 129.27 (C^{8A}); 128.39 (C^{20A}); 128.26 (C^{15A}); 127.35 (C^{9A}); 125.90 (C^{12A}); 123.94 (C^{5A}); 121.25 (C^{3A}); 118.44 ($C^{3'A}$). UV−vis (CH_3CN) λ_{max}/nm (ϵ/M^{-1} cm^{-1}): 252 (43 700), 296 (44 980), 309 (45 570). Anal. Calcd for $C_{44}H_{31}N_4(0.1HSO_4^-, 0.9CH_3CO_2^-)$: C, 81.06; H, 5.02; N, 8.26. Found: C, 80.82; H, 4.84; N, 8.51. CI-MS data: m/z 615 [M^+].

[Ru(tpy-TPH_3^+)$_2$](PF_6)$_4$, (P0A$_2$/Ru). $RuCl_3 \cdot 3H_2O$ (16 mg, 0.061 mmol) and [H_3TP^+-tpy](BF_4) (87 mg, 0.13 mmol, 2.1 equiv) were

dissolved in absolute EtOH (10 mL) and heated for 0.5 h. 1,2-Ethanediol (20 mL) and sodium ascorbate (121 mg, 0.612 mmol, 10 equiv/Ru) were then added, and the resulting mixture was heated at 110 °C for 21 h under an inert atmosphere. At room temperature, while stirring, a solution of NH_4PF_6 (199 mg, 1.22 mmol, 20 equiv/Ru) in distilled H_2O (25 mL) was added to precipitate the complex, which was then filtered off and washed successively with H_2O, EtOH, and Et_2O. The orange product was purified by column chromatography over basic alumina using an eluent mixture of CH_2Cl_2/acetone from 100:0 to 0:100. A recrystallization from acetone/$CHCl_3$ mixture led to red-orange crystals (85 mg; yield 78%). Anal. Calcd for $C_{76}H_{54}N_8RuP_4F_{24}\cdot H_2O$: C, 51.33; H, 3.17; N, 6.30. Found: C, 51.30; H, 3.02; N, 6.24.

[(tpy)Ru(tpy-TPH$_3^+$)](PF$_6$)$_3$, (P0A/Ru). (tpy)$RuCl_3$ (65 mg, 0.147 mmol) and [H_3TP^+-tpy](BF_4) (118 mg, 0.177 mmol, 1.2 equiv) were suspended in 1,2-ethanediol (20 mL) in the presence of sodium ascorbate (292 mg, 1.47 mmol, 10 equiv/Ru) and heated at 120 °C for 17 h under an inert atmosphere (Ar). Afterward, while vigorously stirring, EtOH (10 mL) and H_2O (20 mL) were added together with NH_4PF_6 (481 mg, 2.95 mmol, 20 equiv/Ru) for the precipitation of the complex. The product was filtered off and washed successively with H_2O, EtOH, and Et_2O to give an orange product which was purified by column chromatography over basic alumina using an eluent of increasing polarity, i.e., a mixture of CH_2Cl_2/acetone from 100:0 to 0:100. Recrystallization in acetone/$CHCl_3$ afforded a dirty orange microcrystallized product (148 mg; yield 77%). Anal. Calcd for $C_{53}H_{38}N_7RuP_3F_{18}$: C, 48.63; H, 2.93; N, 7.49. Found: C, 48.66; H, 2.93; N, 7.34.

[Ru(ptpy-TPH$_3^+$)$_2$](PF$_6$)$_4$, (P1A$_2$/Ru). A mixture of $RuCl_3\cdot 3H_2O$ (18 mg, 0.069 mmol), [H_3TP^+-ptpy](0.1HSO_4^-, 0.9OAc^-) (98 mg, 0.145 mmol, 2.1 equiv, dissolved in 5 mL of CH_2Cl_2), sodium ascorbate (136 mg, 0.688 mmol, 10 equiv/Ru), and 1,2-ethanediol (15 mL) was heated to 110 °C for 18 h under an Ar atmosphere. The reaction medium was cooled to room temperature, and then EtOH (10 mL), distilled H_2O (25 mL), and a large excess of NH_4PF_6 (225 mg, 1.376 mmol, 20 equiv/Ru) were added while vigorously stirring, resulting in the precipitation of the complex which was filtered off, successively washed with H_2O, EtOH, and Et_2O, and air-dried. The crude orange powder was subsequently purified by column chromatography over basic alumina, eluting first with CH_2Cl_2/acetone using a gradient of acetone (up to 100%), second with CH_3CN, and finally with a saturated CH_3CN solution of NH_4PF_6. After removal of the salt by precipitating twice the complex in EtOH, the product was recrystallized by slow vapor diffusion of Et_2O in a solution of the product in CH_3CN, giving fine orange needles (48 mg; yield 36.5%). Anal. Calcd for $C_{88}H_{62}N_8RuP_4F_{24}$: C, 55.26; H, 3.27; N, 5.86. Found: C, 55.23; H, 3.23; N, 6.05. HRMS (ES) data: *m/z* 811.62 [M − 2PF_6^-]$^{2+}$; 492.66 [M − 3PF_6^-]$^{3+}$; 333.31 [M − 4PF_6^-]$^{4+}$.

[Os(ptpy-TPH$_3^+$)$_2$](PF$_6$)$_4$, (P1A$_2$/Os). The complex was synthesized and purified following a procedure similar to the one described for the Ru^{2+} analogue, **P1A$_2$/Ru**. A mixture of $OsCl_3\cdot 3H_2O$ (24 mg, 0.068 mmol), [H_3TP^+-ptpy](0.1HSO_4^-, 0.9OAc^-) (98 mg, 0.144 mmol, 2.1 equiv in 5 mL of CH_2Cl_2), sodium ascorbate (136 mg, 0.685 mmol, 10 equiv/Os), and 1,2-ethanediol (15 mL) was heated to 110 °C for 20 h under inert atmosphere. The final recrystallization gave thin brown needles (50 mg; yield 36.2%). Anal. Calcd for $C_{88}H_{62}N_8OsP_4F_{24}\cdot H_2O$: C, 52.33; H, 3.19; N, 5.55. Found: C, 51.92; H, 2.98; N, 5.55. ES-MS data: *m/z* 1857 [M − PF_6^-]$^+$; 856 [M − 2PF_6^-]$^{2+}$; 522 [M − 3PF_6^-]$^{3+}$; 355 [M − 4PF_6^-]$^{4+}$.

[(Me-ptpy)Ru(ptpy-TPH$_3^+$)](PF$_6$)$_3$, (P1A/Ru). Under Ar, a mixture of (Me-ptpy)$RuCl_3$ (52 mg, 0.098 mmol), [H_3TP^+-ptpy](0.1HSO_4^-, 0.9OAc^-) (80 mg, 0.118 mmol, 1.2 equiv), and sodium ascorbate (194 mg, 0.979 mmol, 10 equiv/Ru) in 1,2-ethanediol (15 mL) was heated at 110 °C for 14 h. To the red-violet solution at room temperature were then added EtOH (15 mL), H_2O (20 mL), and NH_4PF_6 (319 mg, 1.96 mmol, 20 equiv/Ru) so as to precipitate the complex. The solid was filtered off, washed with H_2O, EtOH, and Et_2O, and air-dried. The crude orange powder was subsequently purified accordingly to the procedure described for **P1A$_2$/Ru**, affording the product as fine orange needles (130 mg; yield 89%). Anal. Calcd for $C_{66}H_{48}N_7RuP_3F_{18}\cdot H_2O$: C, 53.08; H, 3.37; N, 6.57. Found: C, 52.98; H, 3.32; N, 6.49. HRMS (ES) data: *m/z* 592.91 [M − 2PF_6^-]$^{2+}$; 346.98 [M − 3PF_6^-]$^{3+}$.

[(Me-ptpy)Os(ptpy-TPH$_3^+$)](PF$_6$)$_3$, (P1A/Os). A procedure similar to that reported for the Ru^{2+} analogue, **P1A/Ru**, was followed. A mixture of (Me-ptpy)$OsCl_3$ (55 mg, 0.089 mmol), [H_3TP^+-ptpy](0.1HSO_4^-, 0.9OAc^-) (72 mg, 0.106 mmol, 1.2 equiv), and sodium ascorbate (176 mg, 0.887 mmol, 10 equiv/Os) in 1,2-ethanediol (15 mL) was heated at 110 °C for 24 h under Ar. The product was finally obtained as thin brown needles (100 mg; yield 69.6%). Anal. Calcd for $C_{66}H_{48}N_7OsP_3F_{18}\cdot 3H_2O$: C, 48.98; H, 3.36; N, 6.06. Found: C, 48.92; H, 3.30; N, 6.06. ES-MS data: *m/z* 1421 (^{192}Os) and 1419 (^{190}Os), [M − PF_6^-]$^+$; 638 [M − 2PF_6^-]$^{2+}$; 376 [M − 3PF_6^-]$^{3+}$.

[(Me$_2$N-ptpy)$_2$Ru](PF$_6$)$_2$, (D$_2$P1/Ru). Under Ar, a mixture of $RuCl_3\cdot 3H_2O$ (56 mg, 0.214 mmol), Me_2N-ptpy (166 mg, 0.471 mmol, 2.2 equiv), and a large excess of sodium ascorbate (424 mg, 2.14 mmol, 10 equiv/Ru) in 1,2-ethanediol (20 mL) was heated at 100 °C for 3 h. To the dark red-violet solution were then added EtOH (20 mL) and NH_4PF_6 (698 mg, 4.28 mmol, 20 equiv/Ru) to precipitate the complex. The solid was filtered off and washed with H_2O, EtOH, and Et_2O. To eliminate highly fluorescent impurities of different solubility, the crude violet powder was first extracted with acetone and the solution poured into a large excess of EtOAc. One of the strongly emitting impurities remained in solution, whereas the complex precipitated as a brown-orange and shimmering microcrystallized compound. The solid thus obtained was filtered off and washed with EtOAc and Et_2O. In a second step, the solid collected was dissolved in a minimum volume of acetone and poured while vigorously stirring into a large volume of EtOH. A precipitate was formed that was filtered off and washed with EtOH and Et_2O. The final recrystallization was achieved by slow vapor diffusion of Et_2O in a solution of the product in CH_3CN, giving dark violet and microcrystallized powder (167 mg; yield 70.6%). Anal. Calcd for $C_{46}H_{40}N_8RuP_2F_{12}\cdot 0.5H_2O$: C, 50.00; H, 3.74; N, 10.14. Found: C, 49.74; H, 3.69; N, 10.12. ES-MS data: *m/z* 403 [M − 2PF_6^-]$^{2+}$.

[(Me$_2$N-ptpy)$_2$Os](PF$_6$)$_2$, (D$_2$P1/Os). A mixture of $OsCl_3\cdot 3H_2O$ (100 mg, 0.285 mmol), Me_2N-ptpy (221 mg, 0.627 mmol, 2.2 equiv), and a large excess of sodium ascorbate (565 mg, 2.85 mmol, 10 equiv/Os) in 1,2-ethanediol (20 mL) was heated at 100 °C for 14 h under Ar. To the dark brown-violet solution at room temperature were then added EtOH (20 mL) and NH_4PF_6 (930 mg, 5.70 mmol, 20 equiv/Os) to precipitate the complex. The solid was filtered off and washed with H_2O, EtOH, and Et_2O. The product was subsequently purified by column chromatography over basic alumina, eluting with a mixture of CH_2Cl_2/acetone using a gradient of acetone (up to 100%) and finally recrystallized by slow vapor diffusion of Et_2O in a solution of the product in CH_3CN (deep violet color), giving glistening greenish crystals (97 mg; yield 28.7%). Anal. Calcd for $C_{46}H_{40}N_8OsP_2F_{12}$: C, 46.62; H, 3.40; N, 9.46. Found: C, 46.58; H, 3.46; N, 9.58. ES-MS data: *m/z* 1041 (^{192}Os) and 1039 (^{190}Os), [M − PF_6^-]$^+$; 448 [M − 2PF_6^-]$^{2+}$.

[(Me$_2$N-ptpy)Ru(ptpy-Me)](PF$_6$)$_2$, (DP1/Ru). Under Ar, a mixture of (Me-ptpy)$RuCl_3$ (100 mg, 0.188 mmol), Me_2N-ptpy (80 mg, 0.227 mmol, 1.2 equiv), and sodium ascorbate (373 mg, 1.88 mmol, 10 equiv/Ru) in 1,2-ethanediol (20 mL) was heated at 100 °C for 3 h. To the red-violet solution were then added EtOH (20 mL) and NH_4PF_6 (614 mg, 3.77 mmol, 20 equiv/Ru) to precipitate the complex. The solid was filtered off and washed with H_2O, EtOH, and Et_2O. The same purification workup as for **D$_2$P1/Ru** was then performed, with an additional step consisting of column chromatography over basic alumina, eluting with CH_2Cl_2 and acetone and using a gradient of acetone (up to 100%). Recrystallization by slow vapor diffusion of Et_2O in a solution of the product in CH_3CN gave a violet and microcrystallized powder (150 mg; yield 74.6%). Anal. Calcd for $C_{45}H_{37}N_7RuP_2F_{12}$: C, 50.66; H, 3.49; N, 9.19. Found: C, 50.56; H, 3.43; N, 9.04. ES-MS data: *m/z* 921 [M − PF_6^-]$^+$; 389 [M − 2PF_6^-]$^{2+}$.

[(Me_2N-ptpy)Os(ptpy-Me)](PF_6)$_2$, (DP1/Os). A mixture of (Me-ptpy)$OsCl_3$ (150 mg, 0.242 mmol), Me_2N-ptpy (102 mg, 0.29 mmol, 1.2 equiv), and sodium ascorbate (479 mg, 2.42 mmol, 10 equiv/Os) in 1,2-ethanediol (20 mL) was heated at 100 °C for 14 h under inert atmosphere. To the dark brown-violet solution were then added EtOH (20 mL) and NH_4PF_6 (789 mg, 4.84 mmol, 20 equiv/Os), leading to the precipitation of the complex. The solid was filtered off and washed with H_2O, EtOH, and Et_2O. The product was subsequently purified by column chromatography over basic alumina. Elution was performed with CH_2Cl_2 and acetone using a gradient of acetone (up to 100%). Finally, recrystallization by slow vapor diffusion of Et_2O in a solution of the product in CH_3CN gave a dark brown and microcrystallized powder (125 mg; yield 44.7%). Anal. Calcd for $C_{45}H_{37}N_7OsP_2F_{12}$: C, 46.75; H, 3.23; N, 8.48. Found: C, 46.72; H, 3.27; N, 8.51. ES-MS data: *m*/*z* 1012 (^{192}Os) and 1010 (^{190}Os), [M − PF_6^-]$^+$; 448 [M − $2PF_6^-$]$^{2+}$.

(Me_2N-ptpy)$RuCl_3$. A mixture of $RuCl_3\cdot 3H_2O$ (200 mg, 0.765 mmol) and Me_2N-ptpy (275 mg in CH_2Cl_2, 1 mL, 0.78 mmol, 1.02 equiv) in EtOH (30 mL) was refluxed for 1 h. At room temperature, the dark precipitate was filtered off, thoroughly washed with H_2O, EtOH, CH_2Cl_2, and Et_2O, and air-dried, giving (Me_2N-ptpy)$RuCl_3$ as a dark brown powder (395 mg; yield 92.2%).

(Me_2N-ptpy)$OsCl_3$. The compound was prepared following the procedure described for **(Me_2N-ptpy)$RuCl_3$**, with $OsCl_3\cdot 3H_2O$ (200 mg, 0.57 mmol) and Me_2N-ptpy (205 mg in CH_2Cl_2, 1 mL, 0.58 mmol, 1.02 equiv) in EtOH (30 mL), refluxed for 1 h. (Me_2N-ptpy)$OsCl_3$ was obtained as a dark brown powder (240 mg; yield 65%).

[(Me_2N-ptpy)Ru(ptpy-TPH_3^+)](PF_6)$_3$, (DP1A/Ru). Under Ar, (Me_2N-ptpy)$RuCl_3$ (100 mg, 0.179 mmol), [H_3TP^+-ptpy](0.1HSO_4^-, 0.9OAc^-) (133 mg, 0.197 mmol, 1.1 equiv), and sodium ascorbate (354 mg, 1.786 mmol, 10 equiv/Ru) in 1,2-ethanediol (18 mL) were heated at 80 °C for 18 h. The complex was precipitated at room temperature by adding to the dark violet solution of EtOH (15 mL), H_2O (20 mL), and NH_4PF_6 (582 mg, 3.57 mmol, 20 equiv/Ru). The solid was filtered off and washed with H_2O, EtOH, and Et_2O. The crude powder in solution in acetone was adsorbed over basic alumina and subsequently column chromatographed, eluting first with CH_2Cl_2 and acetone using a gradient of acetone (up to 100%), second with CH_3CN, and finally with a saturated solution of NH_4PF_6 in CH_3CN. After removal of the salt by precipitating twice the complex in EtOH, the product was recrystallized by slow vapor diffusion of Et_2O in a solution of the product in CH_3CN, giving a red-violet microcrystalline solid (173 mg; yield 64%). Anal. Calcd for $C_{67}H_{51}N_8RuP_3F_{18}\cdot 0.5H_2O$: C, 53.18; H, 3.46; N, 7.41. Found: C, 53.06; H, 3.46; N, 7.39. ES-MS data: *m*/*z* 357 [M − $3PF_6^-$]$^{3+}$.

[(Me_2N-ptpy)Os(ptpy-TPH_3^+)](PF_6)$_3$, (DP1A/Os). Under Ar, (Me_2N-ptpy)$OsCl_3$ (145 mg, 0.223 mmol), [H_3TP^+-ptpy](0.1HSO_4^-, 0.9OAc^-) (167 mg, 0.246 mmol, 1.1 equiv), and sodium ascorbate (443 mg, 2.23 mmol, 10 equiv/Os) in 1,2-ethanediol (20 mL) were heated at 100 °C for 14 h. The purification was performed as for **DP1A/Ru**, giving a brown-violet microcrystallized solid (143 mg; yield 39.5%). Anal. Calcd for $C_{67}H_{51}N_8OsP_3F_{18}\cdot 1.5H_2O$: C, 49.66; H, 3.36; N, 6.92. Found: C, 49.59; H, 3.34; N, 6.95. ES-MS data: *m*/*z* 1450 (^{192}Os) and 1448 (^{190}Os), [M − PF_6^-]$^+$; 652 [M − $2PF_6^-$]$^{2+}$; 386 [M − $3PF_6^-$]$^{3+}$.

Acknowledgment. We are indebted to Dr. Kurt Schenk for his support regarding X-ray crystallography and Dr. Isabelle Corriera for ROESY experiments.

Supporting Information Available: ORTEP drawings along with related numbering schemes, tables of crystal data, structure solution and refinement, atomic coordinates, bond lengths and angles, and anisotropic thermal parameters for [H_3TP^+-tpy]-(BF_4)·0.5$CH_3CO_2C_2H_5$, [H_3TP^+-ptpy](anion)·solvent, **P0A/Ru**·0.8CH_3CN·0.5H_2O, and **P1A$_2$/Ru**; plot of $d(C_{Ar1}-N_{py+})$ as a function of $\theta 1$; ^{1}H and ^{13}C NMR data along with related assignments for all inorganic compounds as well as a selected part of the ROESY spectrum of a CD_3CN solution of **P0A/Ru**; figure showing the ground-state electronic spectra of the P0/Ru series of complexes (PDF). This material is available free of charge via the Internet at http://pubs.acs.org.

JA011069P